https://doi.org/10.5194/gmd-2023-237
Preprint. Discussion started: 10 January 2024

Geoscientific Model Development Discussions

Modelling the water isotopes distribution in the Mediterranean Sea using a high-resolution oceanic model (NEMO-MED12-watiso-v1.0): Evaluation of model results against in-situ observations

Mohamed Ayache[1], Jean-Claude Dutay[1], Anne Mouchet[2], Kazuyo Tachikawa[3], Camille Risi[4], and Gilles Ramstein[1]

[1]Laboratoire des Sciences du Climat et de l'Environnement, CEA-CNRS-Université Paris Saclay, 91191, Gif-sur-Yvette, France
[2]Freshwater and OCeanic science Unit of reSearch (FOCUS), Université de Liège, B-4000 Liège
[3]Aix Marseille Univ, CNRS, IRD, INRAE, Coll France, CEREGE, 13545, Aix-en-Provence, France
[4]Laboratoire de Météorologie Dynamique, IPSL, CNRS, Sorbonne Université, Paris, France

Correspondence: Mohamed Ayache (mohamed.ayache@lsce.ipsl.fr)

Abstract.

Stable water isotopes ($\delta^{18}O_{sw}$ and δD) have been successfully implemented for the first time in a high-resolution model of the Mediterranean sea (NEMO-MED12). In this numerical study, model results are compared with available in-situ observations to evaluate the model performance about the present-day distribution of stable water isotopes and their relationship with salinity on a sub-basin-scale. There is good agreement between the modelled and observed distributions of $\delta^{18}O_{sw}$ in the surface water. The model successfully simulates the observed east-west gradient of $\delta^{18}O_{sw}$ characterising surface, intermediate and deep waters. The results also show good agreement between the simulated δD and the in-situ data. The δD shows a strong linear relationship with $\delta^{18}O_{sw}$ (r^2 = 0.98) and salinity (r^2 = 0.94) for the whole Mediterranean Sea. Moreover, the modelled relationships between $\delta^{18}O_{sw}$ and salinity agree well with observations, with a weaker slope in the eastern basin than in the western basin. We investigate the relationship of the isotopic signature of the $CaCO_3$ shell ($\delta^{18}O_c$) with temperature and the influence of seasonality. Our results suggest a more quantitative use of $\delta^{18}O$ records, combining reconstruction with modelling approaches.

1 Introduction

Because of their conservative behaviour, stable water isotopes (δ^{18} [1] and δD [2]) provide a unique opportunity to assess hydrological processes and study the hydrological cycle in climate system variability. The isotopic composition of seawater ($\delta^{18}O$) is globally linked to salinity ($\delta^{18}O$-S relationship) because $\delta^{18}O$ and salinity are affected by common physical processes (i.e. freshwater fluxes or precipitation-evaporation balance). However, the variation of $\delta^{18}O$ is more complex because the water isotopes are subjected to additional fractionation and transport in the atmosphere (Craig and Gordon, 1965). The driving factors

[1]equation 1
[2]equation 2

https://doi.org/10.5194/gmd-2023-237
Preprint. Discussion started: 10 January 2024


Geoscientific Model Development Discussions

mainly incluce surface fractionation in relation to atmospheric exchange and oceanic mixing processes, but also continental runoff in coastal areas and ice processes (sea ice formation and iceberg runoff) in polar regions. The evaporation process preferentially extracts lighter water molecules, and the remaining evaporated seawater becomes rich in heavier isotopes. In contrast, the input of freshwater-rich in lighter isotopes by precipitation or river runoff, leads to a decrease in the $\delta^{18}O$ and δD values of seawater. Thus, the salinity and the isotopic compositions of oceanic waters are acquired at the surface; the sinking of surface waters to intermediate or deeper layers does not change these parameters, which can remain stable over long distances until they mix with waters with different properties.

Although water isotopes are among the most widely used proxies in climate research, there are still gaps in our understanding of the processes that control their marine distribution. General circulation models (GCMs) allow us to better understand the past variability of water isotopes documented in various archives and to investigate the relationship between water isotopes and different climate variables. The heavy stable isotopes of water (i.e. deuterium and oxygen-18) have been incorporated into both atmospheric models (e.g., Joussaume et al., 1984; Jouzel et al., 1987; Hoffmann et al., 1998; Brown et al., 2006; Risi et al., 2010a, b; Werner et al., 2011) and oceanic models (Schmidt, 1998, 1999; Paul et al., 1999; Delaygue et al., 2000, 2001; Wadley et al., 2002; Xu et al., 2012), and in coupled ocean-atmosphere models (Schmidt et al., 2007; Tindall et al., 2010; Roche et al., 2004; Roche and Caley, 2013; Werner et al., 2016; Cauquoin et al., 2019; Shi et al., 2023). In recent decades, $\delta^{18}O_{sw}$ and δD data have become increasingly important in paleoclimate modelling studies and have been incorporated into global climate models. The isotopic signals are explicitly simulated to compare with observations, to quantify processes affecting reconstructed seawater isotopic compositions (Roche and Caley, 2013; Schmidt et al., 2007). Previous reviews of water isotope measurements and modelling studies (Galewsky et al., 2016; Jones and Dee, 2018; Bowen et al., 2019) have highlighted the importance of understanding spatial and temporal isotopic variability for a quantitative interpretation of its relationship with climate change, and have also shown the potential of $\delta^{18}O$ to characterise individual water masses. However, water isotopes have not been incorporated in a high resolution regional ocean model. Here, we present the first results of a high-resolution regional dynamical model (at 1/12° horizontal resolution) developed for the Mediterranean Sea (Beuvier et al., 2012a).

In the Mediterranean region, net freshwater fluxes at the sea surface, *i.e.*, the difference between evaporation and precipitation, are the main driving factor of the hydrological cycle (Mariotti et al., 2002), and there is no effect of sea ice formation or melting (*i. e.* no freshwater inflow from ice sheets during the recent "present situation" period). This condition provides a unique opportunity to better understand the spatial and temporal variations of water isotopes in a semi-enclosed basin, away from the interference of sea ice which is currently poorly represented in models. The negative balance between net freshwater input and evaporation (P + R - E < 0) leads to an anti-estuarine pattern in the Mediterranean thermohaline circulation system, with a surface input of less saline Atlantic Water (AW) through the Strait of Gibraltar, which is then gradually transformed into saltier water, eventually sinking into the Levantine sub-basin to form Intermediate Levantine Water (LIW) that spreads across the eastern Mediterranean at water depths of between 150 and 700 m until it reaches the Strait of Gibraltar to form the Mediterranean Outflow Water (MOW) (Millot and Taupier-Letage, 2005; Lascaratos et al., 1999). The LIW is one of the main water masses in the Mediterranean Sea (Pinardi and Masetti, 2000), contributing to the formation of the Eastern Mediterranean Deep Water (EMDW) in the Adriatic sub-basin and the Western Mediterranean Deep Water (WMDW) in the Gulf of Lion.

https://doi.org/10.5194/gmd-2023-237
Preprint. Discussion started: 10 January 2024

Geoscientific Model Development Discussions

The Mediterranean Outflow Water (MOW) plays an important role in the North Atlantic overturning circulation, because the excess salt transported by the water mass contributes to increasing the density of the water masses in the convection zones of the deep water formation (Bigg et al., 2003). In the past, the Mediterranean thermohaline circulation has been profoundly altered, notably during sapropel events, when deep-water ventilation was strongly reduced in the eastern basin, that are well documented by water isotopes observations (Rohling et al., 2015 and references therein). Major changes are also possible in the future as a result of global warming (e.g., Somot et al., 2006; Adloff et al., 2015; Pagès et al., 2020). Understanding the processes that control the circulation of the Mediterranean Sea is therefore a major challenge for understanding climate variability in the Mediterranean basin (e.g., Soto-Navarro et al., 2020).

Compared to other large ocean basins, the Mediterranean Sea can be considered ideal to improve our understanding of the processes that influence and drive oxygen isotope variations, and to further develop the existing modelling approach, because (i) the water residence time is relatively short ($\sim$ 100 years; Millot and Taupier-Letage (2005)); (ii) all major forcing mechanisms are present, including air-sea interaction, buoyancy fluxes and wind forcing, with a well-studied salinity and water isotope structure (e.g., Pierre, 1999); (iii) a well marked $\delta^{18}O_{sw}$ of the surface waters of the eastern Mediterranean basin (value up to 2.2 ‰, Gat et al., 1996) has the potential as an oceanographic tracer to trace the process of deep water formation and the thermohaline circulation variability; (iv) a high spatial resolution regional model (NEMO-MED12) is available, which is essential for the simulation of realistic ocean dynamics, and which can then be used for past climate simulation with the adapted coupled regional model (Vadsaria et al., 2020). Over the last decades, considerable progress has been achieved in our understanding of the processes and mechanisms governing the distribution of water isotopes in the Mediterranean Sea, through high quality sampling and measurements (e.g., Gat et al., 1996; Pierre, 1999; LeGrande and Schmidt, 2006). Nonetheless, no specific modelling focused on water isotopes is yet available for the Mediterranean Sea. The aim of this study is to implement water isotopes as passive tracers in the high-resolution dynamical model (NEMO-MED12) in order to prepare a direct evaluation of paloclimate simulation that will then be performed using this modelling platform. We use fluxes from the atmospheric general circulation model (LMDZ-iso, Risi et al., 2010b). Our paper focuses on the simulation of the present-day oceanic distribution of $\delta^{18}O_{sw}$ and δD. We compare model results with existing observations to assess the model's ability to capture the main features of water isotopes distribution in the Mediterranean Sea, as well as the relationship between salinity as a function of $\delta^{18}O_{sw}$ and δD. By combining $\delta^{18}O_{sw}$ and temperature, we are able to calculate equilibrated calcite $\delta^{18}O_c$ values using paleotemperature equations to compare model results with recent biogenic carbonate data. The results are analysed for the eastern (EMed) and western (WMed) basins to investigate the processes leading to the isotopic distribution of $\delta^{18}O$ and δD in the Mediterranean Sea. The knowledge of the present-day variability of the isotopic composition of Mediterranean waters should help further studies dedicated to Mediterranean paleoceanography.

https://doi.org/10.5194/gmd-2023-237
Preprint. Discussion started: 10 January 2024


Geoscientific Model Development Discussions

2 Method

2.1 Circulation and ocean dynamic using the NEMO-MED12 model

The dynamical model is the NEMO (Nucleus for European Modelling of the Ocean) free surface ocean circulation model (Madec and NEMO-Team., 2008) in a regional high-resolution configuration (at 1/12° =∼ 7 km) called NEMO-MED12 (Beuvier et al., 2012b). The NEMO-MED12 domain covers the entire Mediterranean Sea and includes the west of Gibraltar in the Atlantic Ocean (buffer zone) from 30–47º N in latitude and from 11ºW–36º E in longitude, where salinity and temperature (3-D fields) are relaxed to the observed climatology (Beuvier et al., 2012a). Water exchange with the Black Sea is represented as a two-layer flow with net budget estimates from Stanev and Peneva (2002). The dynamical simulation (the circulation fields, i.e. U, V and W) has been forced with atmospheric fluxes from the high-resolution (50 km) ARPERA dataset (Herrmann and Somot, 2008; Herrmann et al., 2010). NEMO-MED12 is forced by ARPERA daily fields of momentum, evaporation and heat fluxes over the period 1958-2013. For the surface temperature condition, a relaxation term to sea surface temperature (SST) from ERA40 is applied for the heat flux (Beuvier et al., 2012b). This term acts as a first-order coupling between the ocean model's SST and the atmospheric heat flux (Barnier et al., 1995), ensuring consistency between these two terms. The value of the relaxation coefficient is spatially constant and is taken to be -40 W m^{-2} K^{-1}, following the CLIPPER Project Team (1999). It corresponds to a 1.2-day restoring timescale for a surface layer of 1 m thickness (Beuvier et al., 2012a).

Numerous studies on ocean dynamics and biogeochemical cycles in the Mediterranean have been carried out using the NEMO-MED12 model (e.g., Brossier et al., 2011; Beuvier et al., 2012b; Soto-Navarro et al., 2014; Ayache et al., 2015a, b, 2016, 2017, 2023; Palmiéri et al., 2015; Guyennon et al., 2015; Richon et al., 2018, 2019). The NEMO-MED12 model represents well the main structures of the Mediterranean thermohaline circulation, with mechanisms having a realistic timescale compared to observations (Ayache et al., 2015a). However, some features of the simulation still need to be improved: for example, the weak formation of the Adriatic deep water (AdDW) as shown using anthropogenic tritium (Ayache et al., 2015a) and CFC simulations (Palmiéri et al., 2015). In the western basin, the WMDW is generally well simulated, but the propagation of the recently ventilated deep water to the south of the basin is underestimated (Ayache et al., 2015a; Palmiéri et al., 2015). All the details of the model and its parameterisations are described separately in (Beuvier et al., 2012b, a; Palmiéri et al., 2015; Ayache et al., 2015a).

2.2 Implementing water isotopes in the NEMO model

Seawater isotopologues ($\delta^{18}O_{sw}$ and δD) were implemented in the regional hi gh-resolution model NEMO-MED12 (release 3.4 and 3.6 of the NEMO model). A detailed description of the source code of the water isotopes package, with a user's guide, are available in the Supplementary Material (cf. Text S1 in the Supplement). The exact version of the model used to produce the results reported in this paper is archived on Zenodo (https://doi.org/10.5281/zenodo.10453745, Ayache et al., 2024, see supplement).

The Hydrogen and oxygen isotope compositions are reported as isotopic ratio anomalies with respect to the Vienna Standard Mean Ocean Water reference value (VSMOW):

https://doi.org/10.5194/gmd-2023-237
Preprint. Discussion started: 10 January 2024

Geoscientific Model Development Discussions

$$\delta^{18}O = \left(\frac{^{18}R}{^{18}R_{VSMOW}} - 1\right) \cdot 10^3, \quad where \ ^{18}R = \frac{^{18}O}{^{16}O} \tag{1}$$

$$\delta D = \left(\frac{^{D}R}{^{D}R_{VSMOW}} - 1\right) \cdot 10^3, \quad where \ ^{D}R = \frac{^{2}H}{^{1}H} \tag{2}$$

where $^{18}R_{VSMOW}$ and $^{D}R_{VSMOW}$ are the SMOW standard ratios for ^{18}O and D respectively. The natural abundances of the oxygen and hydrogen isotopes are ^{16}O:^{17}O: ^{18}O=0.9976: 0.00038: 0.00205, and ^{1}H: ^{2}H (D)= 99.985: 0.00015 (Mook et al. (1974), bouquin AIEA; Gat, 1996).

For simplicity, we explain the implementation of the water isotope in the NEMO-MED12 model using $\delta^{18}O_{sw}$. Equations for δD are readily obtained by replacing the isotopic ratio where relevant. Water isotopes behave as conservative tracers in the ocean; they are only modified by fluxes across open boundaries (Craig and Gordon, 1965; Schmidt, 1998; Delaygue et al., 2000; Roche et al., 2004). It is common to transport the isotopic ratio rather than the individual isotope: e.g. radiocarbon distribution ^{14}C/C in the Mediterranean Sea (Ayache et al., 2017) and $\delta^{18}O$ of precipitation (Risi et al., 2010b). Therefore, the equation governing the transport of the isotopic ratio in the ocean is:

$$\frac{\delta}{\delta t}{}^{18}r + \nabla \cdot (u\,{}^{18}r - K \cdot \nabla {}^{18}r) = 0 \tag{3}$$

where u is the 3-D velocity field, and K is the diffusivity tensor. It should be noted that the isotopic ratio ^{18}r in equation 3 is relative to the total of all isotopic forms. If we neglect the low abundant ^{17}O then the relationship between ^{18}r = ^{18}O/O and ^{18}R = ^{18}O/^{16}O is straightforward.

$$^{18}r = \frac{^{18}R}{(1 + ^{18}R)} \quad and \quad ^{18}R = \frac{^{18}r}{(1 - ^{18}r)} \tag{4}$$

The water isotopes are implemented using the passive tracer engine "TOP: Tracers in Ocean Paradigm" of the NEMO-MED12 ocean model by providing all physical constraints/boundaries of δ^{18}O and δD and pseudo-salinity tracers (see Appendix Text S1). Here, we used the offline coupling mode. In this method, the physical variables i.e., the circulation fields (U, V, W) and mixing coefficients (Kz) are previously computed by the NEMO-MED12 dynamical model (Beuvier et al., 2012a) and used to propagate the tracers in the ocean. The physical forcing fields are read daily and interpolated to give values for each 20 min time step. The same approach has been used to simulate the neodymium budget in the present Mediterranean Sea (Ayache et al., 2023) and the past isotopic distribution of Nd (Vadsaria et al., 2019), the anthropogenic tritium invasion (Ayache et al., 2015a), the distribution of CFCs (Palmiéri et al., 2015) and anthropogenic carbon (Ayache et al., 2017). The ocean isotopic ratios are initially set to their standard values: $\delta^{18}O_{sw}$ = 1.5 ‰ and δD =8 ‰, and the pseudo-salinity tracer is set to 37 PSU (after many sensitivity test simulations based on in-situ observations, not shown here). All output fields in Tab S2. are routinely calculated.

https://doi.org/10.5194/gmd-2023-237
Preprint. Discussion started: 10 January 2024

Geoscientific Model Development Discussions

2.3 Atmospheric fluxes and river runoff in un-coupled mode

The boundary conditions at the ocean-atmosphere interface over the Mediterranean regions for the water isotope simulation ($\delta^{18}O$ and δD) are given by the isotopic version of the atmospheric model with a comprehensive representation of water isotopes (LMDZ-iso GCM; Risi et al. (2010b)). They consist of climatological gross fluxes of evaporation and precipitation with their isotopic composition (Fig. 1). This ensures consistency between water (evaporation and precipitation) and isotopic fluxes, which is of primary importance here, since their balance generates our tracer distribution, as discussed in Delaygue et al. (2000) and Juillet-Leclerc et al. (1997).

Here we force the simulations from the global isotopic atmospheric model LMDZ-iso (Risi et al., 2010b), which is available with two horizontal resolutions; on a coarse latitude–longitude grid R96 (2.5°×3.75°), and on a higher spatial resolution R144 grid (1.27° × 2.5°), the vertical grid of LMDZ-iso extends over 39 layers. We used an AMIP (Atmospheric Model Intercomparison Project) simulation for the period 1990 to 2020, forced by monthly and interannually varying observed SST and sea ice, and a constant CO_2 value of 348 ppm (see Risi et al. (2010b, 2013) for more details on the atmospheric simulation). LMDZ-iso simulates reasonably well the spatial and seasonal variations of both $\delta^{18}O$ and deuterium excess (d-excess= δD – 8* $\delta^{18}O_{sw}$, Dansgaard, 1964; Risi et al., 2010b). These fluxes where carefully interpolated onto the NEMO-MED12 grid (see Fig. 1). It must be acknowledged that the spatial resolution of LMDZ-iso is relatively coarse for the Mediterranean Sea. It was necessary to use low resolution forcing on the simulated isotopic composition concentration, because no higher resolution atmospheric isotopic model simulations similar to the dynamical forcing of NEMO-MED12 dynamical simulation (50km) are available at the moment. We therefore performed some sensitivity tests of the results by changing the horizontal resolution of LMDZ-iso between R96 and R144 (cf. Section 4). The impact of this low resolution on the simulated isotopic composition is limited because we used pre-calculated dynamical fields of the NEMO-MED12 model (in off-line mode) forced by a higher resolution atmospheric model (50 km) ARPERA dataset (Beuvier et al., 2012b; Herrmann and Somot, 2008; Herrmann et al., 2010).

Isotopes are included in the river discharge of the land surface model ORCHIDEE (Risi et al., 2016) but the isotopic version of ORCHIDEE is too old to be coupled with LMDZ-iso. Therefore, as previously done in Delaygue et al. (2000) for the global ocean, we used river discharge estimation from observations and attributed the isotopic composition of precipitation at the river mouth. River inputs are introduced as freshwater source at river mouths in the surface layer (Fig. 1g, h, i). We used the climatological mean of the interannual dataset of Ludwig et al. (2009) to compute monthly runoff values of the 33 main river mouths covering the entire Mediterranean draining basin (RivDis dataset Vörösmarty et al., 1996).

The values of the inputs of the other rivers are averaged in each Mediterranean sub-basin and placed as coastal runoff in each MED12 coastal grid point of these sub-basins (Fig. 1g, h, i), as done in Beuvier et al. (2012a) and in Palmiéri et al. (2015). Similarly, since it is difficult to couple the old isotopic version of ORCHIDEE with the current version of LMDZ, we adopt an alternative solution to represent the isotopic flux carried by rivers to the ocean: this flux is calculated as $\mathcal{R}_R = \mathcal{R}_P \times R$ where R is the runoff prepared from the data of Ludwig et al. (2009) and Vörösmarty et al. (1996) (see above) and $\mathcal{R}_P$ is the isotopic ratio in precipitations at the same time and location (Fig. 1) as adapted from Delaygue et al. (2000). The exchange with

https://doi.org/10.5194/gmd-2023-237
Preprint. Discussion started: 10 January 2024

Geoscientific Model Development Discussions

the Atlantic Ocean is performed through a buffer zone between 11°W and the Strait of Gibraltar, where 3-D water isotopes ($\delta^{18}O_{sw}$ and δD) and salinity model fields are relaxed to the observations from the Global gridded data set of oxygen isotopic composition in seawater (LeGrande and Schmidt, 2006) and using global model outputs after multiple sensitivity simulations (not shown here).

Let $\mathcal{E}$, $\mathcal{P}$, $\mathcal{R}$ represent evaporation, precipitation, and run-off, respectively, then the following boundary condition is relevant at the sea surface.

$$\mathcal{F}^{18}O = \mathcal{E}(\mathcal{R}_s - \mathcal{R}_E) - \mathcal{P}(\mathcal{R}_S - \mathcal{R}_P) - \mathcal{R}(\mathcal{R}_S - \mathcal{R}_R) \quad (5)$$

where $\mathcal{R}_S$ is the isotopic ratio of the oceanic surface, $\mathcal{R}_E$, $\mathcal{R}_P$ and $\mathcal{R}_R$ are the isotopic ratios of evaporation (E), precipitation (P) and run-off (R).

2.4 Pseudo salinity in stand-alone ocean model

The water fluxes from the stand-alone experiments with LMDZ-iso are not identical to those constraining NEMO-MED12. Therefore, $\delta^{18}O_{sw}$ or δD computed with the water fluxes obtained with LMDZ-iso would not be consistent with the salinity predicted by NEMO-MED12. For this reason we compute a "pseudo-salinity" S_w (Delaygue et al., 2000; Roche et al., 2004). This additional passive tracer has no effect on ocean dynamics. Its sole purpose is to provide a coherent assessment of the isotopic fields generated by the model. The evolution equation for S_w is given by equation 5 where we replace $\mathcal{R}_s$ by S_w and where a zero salinity is associated to the water fluxes (i.e. $\mathcal{R}_E$, $\mathcal{R}_P$ and $\mathcal{R}_R$ = 0 when solving equation 5 for S_w). This passive tracer, hereafter called 'pseudo-salinity', is calculated "offline". The basic understanding of these atmospheric fluxes, $\mathcal{F}^{18}O$ and $\mathcal{F}^{S}$, is that evaporation tends to increase the surface salinity, and the ^{18}O/^{16}O ratio, in contrast to precipitation and runoff.

2.5 Datasets of $\delta^{18}O_{sw}$ and δD to evaluate the simulation

For comparison with our model results, we used published in-situ data in the Mediterranean Sea (https://data.giss.nasa.gov/cgi-bin/o18data/geto18.cgi) including Epstein and Mayeda (1953), Stahl and Rinow (1973), Pierre et al. (1986), Gat et al. (1996), and Pierre (1999). We also used the global gridded data set of oxygen isotopic composition in seawater from (LeGrande and Schmidt, 2006) to compare the observed and modelled large-scale oceanic $\delta^{18}O_{sw}$ distribution (i.e., the east-west gradient). While δD observations in Mediterranean waters are not as widespread as $\delta^{18}O_{sw}$, there are some data available in the western basin to validate our simulations. For this study we consider δD measurements from Gat et al. (1996).

3 Results

3.1 Simulated present-day distribution of $\delta^{18}O_{sw}$

As a preliminary assessment of our model results, we evaluated the spatial distribution of $\delta^{18}O_{sw}$ in surface waters, zonal vertical sections and basin average vertical profiles (see Table 1 and Fig. 2) forced by the coarse-resolution version (R96) of

https://doi.org/10.5194/gmd-2023-237
Preprint. Discussion started: 10 January 2024

Geoscientific Model Development Discussions

the LMDZ-iso model. The EMed is clearly enriched by more than 0.45 ‰ (see Table 1) compared to the WMed. The largest variation of $\delta^{18}O_{sw}$ of the water is simulated in the surface waters with a strong east-west gradient (Fig. 2a); the $\delta^{18}O_{sw}$ value is up to 2 ‰ in the EMed, but only 1.55‰ in the western Mediterranean. This trend reflects the east-west gradient of oceanic evaporation, which distinguishes the higher evaporation in the EMed than in the WMed (Fig. 1). The $\delta^{18}O_{sw}$ distribution shows a north-south enhancement in the eastern basin (Fig. 2a) with less enriched surface water in the Aegean and Adriatic basins, two regions characterised by active vertical mixing homogenising the water column, and a relatively high contribution of river discharge to this region (e.g. the Po River in the Adriatic basin). The vertical $\delta^{18}O_{sw}$ distributions are well captured by the model as shown in the west-to-east section and the vertical profile across the Mediterranean (Fig. 2). The intermediate waters (200-800 m depth) form a more homogeneous layer relative to the surface waters. However, the $\delta^{18}O_{sw}$ values decrease towards the west by 0.35‰ at most, which is due to gradual dilution by mixing with the deeper water masses and the Atlantic water. The deep water exhibits homogeneous $\delta^{18}O_{sw}$ values similar to the simulated values in the intermediate water, indicating well-ventilated conditions due to active winter convection.

Comparison of the model output with in situ data shows that the model reproduces well the observed east–west gradient that characterises the surface waters (Fig. 2a, Table 1), and correctly reproduces the zonal gradients observed in the intermediate and deep waters (Fig. 2b and 2c). The simulated mean vertical profile of $\delta^{18}O_{sw}$ is consistent with the observations in the western basin of $\delta^{18}O_{sw}$ values (Fig. 2d). The spreading of Atlantic water in the surface of the Alboran basin is well reproduced in the simulation (Fig. 2a, 2d). In the eastern basin, the highest value of $\delta^{18}O_{sw}$ is well reproduced in the simulation, but the model largely underestimates the mean values of the observations in the intermediate and deep waters (Fig. 2e, 2e). This offset is related to the weak formation of the simulated EMDW in the Adriatic sub-basin, as already noted by Ayache et al. (2015a); Palmiéri et al. (2015). To further evaluate the relationship between the in situ data and the simulated $\delta^{18}O_{sw}$, the longitudinal distribution of $\delta^{18}O_{sw}$ is examined for each basin (Fig. 3b, 3c). A pronounced longitudinal gradient is found for simulated and observed $\delta^{18}O_{sw}$ values, with more enriched values in the EMed (between -6°E and 11°E) and more depleted values in the WMed (between 27°E and 36°E) with an intermediate value in the central basin (Fig. 3b, 3c). The observed salinity agrees well with the simulation results (Fig. 3), in contrast to the highly variable in situ $\delta^{18}O_{sw}$ values.

3.2 The $\delta^{18}O_{sw}$-salinity relationship in the Mediterranean waters

The lower two panels in Fig. 3 show the depth profiles of salinity in relation to $\delta^{18}O_{sw}$ from in-situ data (Fig. 3d) and model output (Fig. 3e) forced by the coarse-resolution version (R96) of the LMDZ-iso model. The more evaporated water in the eastern basin (salinity up to 38.9) matches well with more enriched water ($\delta^{18}O_{sw}$ above 1.98 ‰), especially at intermediate depths (300-700 m) corresponding to the LIW layer. The decrease in $\delta^{18}O_{sw}$ and salinity in the deep water is well captured by the model (Fig. 3c, 3d, 3e). However, the model tends to overestimate the value of $\delta^{18}O_{sw}$ associated with a lower salinity in the WMed (salinity = ∼36.4), i.e. the salinity of the inflowing Atlantic waters (Fig. 3c and Fig. 3e).

To further analyse the relationship between $\delta^{18}O_{sw}$ and salinity, we plot the regression slope of $\delta^{18}O_{sw}$ versus salinity for the available in situ data (Fig.4a, b, c) and from the model output (Fig.4 d, e, f). There is a significant positive correlation between salinity and $\delta^{18}O_{sw}$ from the model results (r^2 = 0.82) and from the in-situ data (r^2= 0.60) for the whole Mediterranean

https://doi.org/10.5194/gmd-2023-237
Preprint. Discussion started: 10 January 2024


Geoscientific Model Development Discussions

Sea. EMed shows the weakest correlation between salinity and $\delta^{18}O_{sw}$ (r^2 = 0.20, Fig. 4c). The whole set of in-situ data values measured in the Mediterranean waters defines the following linear equation: $\delta^{18}O_{sw}$ = 0.29S – 9.46 (Fig. 4a); the equation becomes: $\delta^{18}O_{sw}$ = 0.26S – 8.60 in the WMed and $\delta^{18}O_{sw}$ = 0.25S – 8.19 in the EMed (Fig. 4b, 4c). The difference between the two equations remains fairly small, with a similar slope in the EMed basin and different intercepts. The model simulated a similar slope to in-situ data throughout the basin ($\delta^{18}O_{sw}$ = 0.25S - 8.01) and the zonal trend is comparable to observation (0.25 and 0.26 for the WMed and the EMed, respectively; Fig. 4e and 4f). Pierre (1999) estimated a similar slope (0.25) for the whole Mediterranean water and 0.27 in the Alboran basin (western basin). Fig. 5a displays the temporal distribution of the $\delta^{18}O_{sw}$-salinity slope in Mediterranean surface water, computed using simulated climatology over last 30 years. Low values (around 0.3, Fig. 5) as well as a weak correlation (0.24, Fig. 4f) were calculated in the eastern basin. High values of slope are simulated in the western basin (> 0.5, Fig. 5a) especially in the Alboran basin which is influenced by Atlantic water characterised by a $\delta^{18}O_{sw}$-S slope of 0.48 (Laube-Lenfant, 1996; Pierre, 1999). While this simulated longitudinal trend appears to agree with observations (Fig. 4 and 5), it is important to note that there are some additional longitudinal variations in slope, particularly in the Aegean Sea and south-easternmost part of the Levantine basin. Fig. 5b displays the spatial $\delta^{18}O$-salinity slope from the model outputs. For each grid point, it is computed as the slope of the $\delta^{18}O_{sw}$ to salinity linear regression, based on the simulated surface values from the 12 surrounding grid points. The mean slope of the spatial regression ($\sim$ 0.3) is relatively similar to the mean value of temporal regression (Fig. 5a). However, the slope based on spatial regression shows greater variation, mainly due to the oceanic circulation, particularly in areas of high mesoscale activity (i.e. the Algerian and Levantine basins), with potentially greater transport/change in salt and water content in the water column caused by the oceanic mesoscale eddies. Finally, using the multi-scatter plot shown in Fig.6, a quantitative comparison was performed between in-situ data and model outputs in the surface layer. A significant correlation was obtained: r^2 values are 0.66 and 0.68 for the whole basin with the LMDZ-iso "96" and "R144", respectively. This shows that the $\delta^{18}O_{sw}$ distribution is globally well simulated by the model. However, neither LMDZ-iso "96" nor "R144" reproduce the highest values of $\delta^{18}O_{sw}$ observed in the Mediterranean Sea (up to 2.4 ‰ as measured by Gat et al. (1996)). Hence, the results of the model are very close between these two horizontal resolutions (R96 and R144) of the LMDZ-iso atmospheric model (Fig.6).

3.3 Present-day distribution of deuterium (δD) and d-excess

Since identical boundary fluxes (precipitation, evaporation and river runoff) drive both $\delta^{18}O_{sw}$ and δD isotopes in the surface water, the zonal gradient patterns between EMed and WMed are strikingly similar (Fig. 7), with the most enriched areas (δD values >= 8 ‰) located in the more evaporated EMed basin and the most depleted areas in the WMed basin (especially the Alboran basin with δD values <= 6 ‰). As for the $\delta^{18}O_{sw}$, the δD values are lower in the Aegean basin, which may be related to a relatively high fresh water contribution (P and R) and an active vertical mixing. The spatial structures of δD simulated by the model are consistent with the observations available in the EMed (Fig. 7) with values slightly higher than in situ data in the surface and intermediate waters. The distributions are more uniform in the deep water. Simulated δD exhibit a linear relationship with $\delta^{18}O_{sw}$ (Fig. 8a), and salinity (Fig.8b) with a significant correlation (r^2=0.98 and 0.94, respectively). δD observations in the Mediterranean are not as extensive as those of $\delta^{18}O_{sw}$, with data only available in the eastern basin (Gat

https://doi.org/10.5194/gmd-2023-237
Preprint. Discussion started: 10 January 2024

Geoscientific Model Development Discussions

et al., 1996). Therefore, there are currently not enough data to constrain and validate our δD simulation as shown in Fig. 8c, where a weak correlation (r^2 = 0.25) was found between the few data available in the eastern basin and δD simulated in the same data location.

The deuterium excess "d-excess" (d-excess= δD - 8* $\delta^{18}O_{sw}$, Dansgaard, 1964) reflects the relationship between the isotopic ratios of hydrogen and oxygen. This indicates the kinetic (non-equilibrium) fractionation effects that occur when water is evaporated from oceanic regions (Dansgaard, 1964). The simulated mean surface water d-excess values range from -4.4‰ to -1.5 ‰, with relatively small variations (variance = -0.27 ‰), and a clear negative shift in simulated d-excess values was observed across the basin (Fig. 9). The WMed basin is enriched in d-excess compared to the EMed basin, and the regions with the lowest d-excess are located in the Levantine sub-basin. Unfortunately, observational data with simultaneous measurements of $\delta^{18}O_{sw}$ and δD are scarce. Consequently, the simulated D-excess values cannot be constrained and validated by observations. However, the model results show an increase in d-excess for water masses with higher $\delta^{18}O_{sw}$ depletion, as suggested by Xu et al. (2012) using the MPI-OM model simulating water isotope variation on a global scale. These negative values are generally in accordance with the positive values of deuterium excess in atmospheric water vapor and precipitation observed and simulated in this region, associated with the dryness of near-surface air (Pfahl and Wernli, 2008).

3.4 Variations of $\delta^{18}O_{calcite}$ in the Mediterranean Sea

A useful tool for reconstructing past climate is the isotopic composition of foraminiferal shells from sediment cores (Shackleton, 1967). However, due to temperature-dependent fractionation, the isotopic signature of the $CaCO_3$ shell ($\delta^{18}O_c$) differs from $\delta^{18}O_{sw}$. The $\delta^{18}O_c$ values depend on both $\delta^{18}O_{sw}$ and seawater temperature at calcification depth. For planktonic foraminifera, the isotopic fractionation relationships during calcification can be assumed to be represented by an equation for equilibrated calcite. We used a paleotemperature equation for inorganic calcite by Kim and O'Neil (1997) modified by Bemis et al. (1998), with the use of the 0.27 ‰ correction from VSMOW (Vienna Standard Mean Ocean Water) to VPDB (Vienna Pee Dee Belemnite) conversion.

$$\mathcal{T} = 16.1 - 4.64(\delta^{18}O_c - \delta^{18}O_{sw}) + 0.09(\delta^{18}O_c - \delta^{18}O_{sw})^2 \tag{6}$$

$$\delta^{18}O_c(VPDB_{‰}) = (\delta^{18}O_{sw}(VSMOW_{‰}) - 0.27) + \frac{4.64 - \sqrt{21.53 - 0.36(16.1 - \mathcal{T}_{^oC})}}{0.18} \tag{7}$$

The relationship of $\delta^{18}O_c$ with temperature and the influence of seasonality are shown in Figure 10. The mean annual $\delta^{18}O_c$ values for surface seawater were computed using the model outputs of surface $\delta^{18}O_{sw}$ and surface water temperature. The simulated annual mean $\delta^{18}O_c$ vary from -0.8 to 2 ‰ in the surface (Fig. 10b), with higher values in the northern part of the Mediterranean and lower values near the southern coast. This latitudinal gradient of $\delta^{18}O_c$ is clearly different from the zonal pattern of $\delta^{18}O_{sw}$ (Fig. 2a) and is related to the effect of temperature (Fig. 10c). Considering this strong temperature dependency, the seasonal variability of $\delta^{18}O_c$ was examined (Fig. 10d). The highest simulated $\delta^{18}O_c$ values were obtained for

https://doi.org/10.5194/gmd-2023-237
Preprint. Discussion started: 10 January 2024

winter (February, March) and the lowest values for summer/autumn. The $\delta^{18}O_c$ calculated from in situ $\delta^{18}O_{sw}$ and measured seawater temperature show the same seasonal trend (Fig. 10e). Even if the available observational data do not cover all the months of the year, our results indicate the importance of temperature effects on $\delta^{18}O_c$ in the Mediterranean Sea. We note here that seasonal variation of $\delta^{18}O_{sw}$ is small in the surface layer of both the eastern and the western basins (see Fig. A1 in appendix). The $\delta^{18}O_c$ variation is mainly localised in surface and intermediate waters (first 300m depth) (Fig. A2 in appendix). The comparison of simulated and observed $\delta^{18}O_c$ (0-50 m depth) shows strong positive correlation with a similar range of variability (between -0.22 and 1.91 ‰ from the model output, and between -0.82 and 1.97 from the in-situ data) as shown in Fig. 10f.

4 Discussion

This study provides the first simulation of the water isotopes ($\delta^{18}O_{sw}$ and δD) in the Mediterranean Sea covering the entire basin. These two tracers were implemented in the high-resolution regional model NEMO-MED12. New insights into the distribution of water isotopes and their relation to salinity in the Mediterranean Sea were obtained by comparing this numerical study with in-situ data. Analysis of the results from an oceanic point of view shows good agreement with the in-situ data, opening up a range of possibilities for long-term palaeoclimate simulations in this basin and for the use of this modelling approach in coupled ocean-atmosphere models. The inputs and boundary conditions $\delta^{18}O_{sw}$ and δD were taken from a global atmospheric model with a low resolution and have been tested for the first time in this study with a regional model at a high resolution. Both observed $\delta^{18}O_{sw}$ and δD show a pronounced east-west gradient, characterised by more enriched water in the eastern basin than in the western basin. This gradient is well captured by the model, and is in good agreement with the available in-situ data. It is not possible to constrain and validate the δD simulation due to the limited number of δD observations. Thus, our discussion below focuses on the results of the $\delta^{18}O_{sw}$ simulation.

A significant correlation between model output and in-situ data (r^2 = 0.68, Fig. 6b) was obtained over the whole basin, with a higher correlation in the WMed basin than in the EMed basin. Our model also successfully simulates the observed vertical distribution of the water isotope composition of the Mediterranean water masses (Fig. 2, Fig. 7). Despite a slight bias in EMed due to the previously reported weak formation of AdDW, the vertical distribution compares favourably with the available in-situ data. Some improvements are still needed in certain aspects of the simulation. The model largely underestimated the mean $\delta^{18}O_{sw}$ values of observations in intermediate and deep waters, and failed to simulate the highly enriched water in the eastern basin (up to 2.4, by ‰ Gat et al. (1996)). This inconsistency should be investigated in a fully coupled ocean-atmosphere model with a higher horizontal/vertical resolution of the atmospheric model. The advantage of using a coupled model lies in the consistent simulation of changes in the different components of the model (for instance between the precipitation over land, the ocean variability and runoff input from the land), and more realistic ocean-atmosphere feedbacks in the coupled model (Bretherton and Battisti, 2000; Schmidt et al., 2007).

The main difference between the data and the numerical simulations is the smaller amplitude of $\delta^{18}O_{sw}$, particularly in the eastern basin. This discrepancy can be explained in two ways. First, this may be due to the low spatial resolution of the isotope

https://doi.org/10.5194/gmd-2023-237
Preprint. Discussion started: 10 January 2024

forcing. Vadsaria et al. (2020) showed that high resolution ($\sim$ 30 km of the atmospheric model) is critical to accurately capture the synoptic variability needed to initiate the formation of the intermediate and deep waters of the Mediterranean thermohaline circulation. Due to the peculiarities of the atmospheric circulation (high wind gusts in winter) and the oceanic circulation (deep convection) in this intercontinental basin, high spatial resolution forcings are needed (Li et al., 2006). Nevertheless, a change in the horizontal resolution of the LMDZ-iso atmospheric model (from R96 to R144, Fig. 6) does not improve the model results, and the model does not simulate the highest values of $\delta^{18}O_{sw}$ observed by Gat et al. (1996) in the eastern basin at either resolution. It is possible that there is a certain threshold of spatial resolution below which the simulation is improved by a finer resolution. Unfortunately, LMDZ-iso simulations at resolutions finer than R144 are not yet available to test this hypothesis.

The second hypothesis is that the discrepancy is due to the physics of the atmosphere, which is independent of the horizontal resolution. In parallel with the too low $\delta^{18}O_{sw}$ in the western part of the basin, LMDZ-iso underestimates the depletion and d-excess of precipitation and vapour in this region (Risi et al., 2010a). These discrepancies in LMDZ-iso are consistent with the insufficient near-surface air dryness. The underestimated dryness would lead to a lower surface evaporative flux in LMDZ-iso, leading NEMO-MED12 to underestimate evaporative enrichment of surface water. In addition, the underestimation of water vapour depletion in the LMDZ-iso leads to an overestimation of evaporative flux (Craig and Gordon, 1965), which in turn leads to a further underestimation of evaporative enrichment of surface water by NEMO-MED12. The underestimation of the dryness in LMDZ-iso could be due to insufficient vertical resolution (Risi et al., 2012) or to a misrepresentation of shallow convection in this region (Hourdin et al., 2015). Such a discrepancy is not observed in the salinity data. In order to obtain larger spatial coverage, we used $\delta^{18}O_{sw}$ obtained in the 1971 to 1990 period in addition to two data points acquired in 1949. Therefore, it is not impossible that temporal variation of $\delta^{18}O_{sw}$ and different data quality with time could induce further scatter. Despite the smaller range of the $\delta^{18}O_{sw}$, our parameterisation produced realistic general features of spatial distribution, particularly zonal trends in surface water. The results suggest that this approach can be used to generate water isotopic simulations with adequate validity at decadal time scales (i.e. 50 years of simulation), opening up the prospect of simulations at longer time scales in the context of palaeoclimate studies.

Mediterranean regional climatic conditions (i.e. excess of evaporation over precipitation) shape a specific relationship in surface waters between observed salinity and $\delta^{18}O_{sw}$ values, characterised by a $\delta^{18}O_{sw}$-S slope of 0.25, much lower than the slope value of 0.45 obtained in Atlantic surface waters (Pierre, 1999). Our results are consistent with these findings: $\delta^{18}O_{sw}$ shows a linear relationship with salinity, and the simulated slope of $\delta^{18}O_{sw}$ with salinity (0.28) is very similar to that calculated by Pierre (1999) using in situ observations. The model simulated similar differences between EMed and WMed, with a steeper slope in WMed as computed using in-situ data. It is not surprising that there is a high correlation between these two fields, since the processes that affect $\delta^{18}O_{sw}$ at the surface are also those that affect surface salinity. Nevertheless, especially in areas of high mesoscale activity (e.g. the Algerian Basin), the spatial slope $\delta^{18}O_{sw}$-S of our simulation shows strong variations. The slope is therefore not homogeneous, but depends on the local climate conditions (wind speed, temperature, etc.). It is well documented that mesoscale eddies can transport water, heat, salt and other tracers as they spread in the ocean, influencing water column properties and biological activities (Chelton et al., 2011; Dong et al., 2014).

https://doi.org/10.5194/gmd-2023-237
Preprint. Discussion started: 10 January 2024

The simulated δD- $\delta^{18}O_{sw}$ relationship provides a realistic d-excess surface field. A comparison between data and model is not possible due to the lack of d-excess field data for the Mediterranean. However, the modelled d-excess is consistent with other modelling studies (e.g. Xu et al., 2012) which show an increase in d-excess for water masses more depleted in $\delta^{18}O_{sw}$. Our simulations show similar negative d-excess values for the whole Mediterranean basin. Thus, assuming that the atmospheric d-excess signature is largely dominated by non-equilibrium isotope fractionation during evaporative processes of marine surface waters (Dansgaard, 1964; Gat et al., 1994), the remaining surface waters should have a negative d-excess value as simulated by our model.

An interesting tool for mapping potential changes in the circulation over time could be a data-model comparison exercise for the $\delta^{18}O$ of calcite in past climates. We are able to calculate $\delta^{18}O_c$ and compare our model results with $\delta^{18}O_c$ calculated from in-situ data, since water temperatures and $\delta^{18}O_{sw}$ are explicitly simulated by our model (see Sec 3.4). The results show that the surface $\delta^{18}O_c$ distributions derived from the model results are consistent with the general spatial pattern of $\delta^{18}O_c$ measurements in the present-day situation. Higher values of $\delta^{18}O_c$ are simulated mainly in the northern part of the Mediterranean as compared to the southern part. The difference between $\delta^{18}O_{sw}$ and $\delta^{18}O_c$ is clearly related to the Mediterranean temperature pattern, with a high negative correlation, especially in the surface layer. $\delta^{18}O_c$ also shows significant seasonal variability, with the highest simulated values in winter and the lowest in summer/autumn, consistent with the seasonal temperature cycle.

To extend this study, certain sensitivity tests/modelling developments must be performed. For the present-day situation, it would be useful to evaluate the influence of different forcing factors on the distribution of water isotopes in the Mediterranean (e.g. the influence of the inflow/outflow from the Atlantic at the Strait of Gibraltar, the influence of surface runoff, etc.). In our experimental set-up, river runoff is computed by considering the isotopic signature of precipitation. This assumption can lead to an unrealistic isotopic composition of the river runoff. Future studies will improve the representation of water isotopes in river runoff using a coupled ocean-atmosphere-land model. For past climates such as the Holocene (i.e. sapropels events), appropriate oceanic circulation and atmospheric fluxes could be combined to estimate differences with the present-day situation. This could help to test and better understand the reconstructed past data. The use of transient simulation offers an interesting test-bed to progress on this issue, especially to evaluate the Mediterranean circulation sensitivity to hydrological/thermal perturbation during the most recent Holocene sapropel S1 (10.5 to 6.1 cal ka BP) and the last interglacial sapropel S5 (128-122 ka, Grant et al., 2016) which occurred under warm conditions with strong seasonality and a high sea level stand.

5 Summary and conclusions

Here, for the first time, stable water isotopes were successfully implemented in a high-resolution regional model of the Mediterranean (called NEMO-MED12-watiso-v1.0) forced by the atmospheric model LMDZ-iso. The isotopic composition of seawater $\delta^{18}O_{sw}$ and δD is simulated explicitly by the oceanic model. The model successfully simulates the observed basin-scale pattern of $\delta^{18}O_{sw}$ and E-W gradients in surface water, evidencing the larger degree of evaporation of surface waters in the eastern basin. It also successfully reproduces the vertical distribution of $\delta^{18}O_{sw}$ in Mediterranean waters masses. Furthermore, the simulated $\delta^{18}O_{sw}$-salinity relationships are also in good agreement with the data, with a smaller slope in the EMed than in the

https://doi.org/10.5194/gmd-2023-237
Preprint. Discussion started: 10 January 2024


Geoscientific Model Development Discussions
Open Access
EGU

WMed, and a slope of 0.25 across the basin. The modelled d-excess values are in good agreement with other modelling studies, with an enhancement of d-excess for water masses depleted in $\delta^{18}O_{sw}$. Such negative d-excess values are found throughout the Mediterranean Sea in our simulation results. We examine the relationship of $\delta^{18}O_c$ with temperature and the influence of seasonality. The gradient of $\delta^{18}O_c$ is clearly different from the pattern of $\delta^{18}O_{sw}$ due to the effect of temperature, with the highest values obtained in winter and the lowest values in summer/autumn.

Improvements are needed in certain aspects of the simulation. A global atmospheric model simulation (LMDZ-iso) with a relatively coarse resolution was used for the isotopic forcing fluxes of precipitation and evaporation. In order to generate steeper gradients in the hydrological cycle variables over the Mediterranean basin (evaporation, precipitation) and to improve the isotopic simulation of the present study, a higher spatial resolution (< 50 km) may be required. The use of a coupled system would provide more physical coherence between atmosphere, land and ocean components and could allow a more reliable simulation of Mediterranean water isotopes. Present-day climate conditions were the focus of this first evaluation of the new stable water isotope package implemented in the NEMO-MED12 model. The model will then be used for different palaeoclimatic conditions to improve our knowledge of past marine isotopic changes and to use it in palaeoclimate reconstructions.

https://doi.org/10.5194/gmd-2023-237
Preprint. Discussion started: 10 January 2024

Geoscientific Model Development Discussions

References

Adloff, F., Somot, S., Sevault, F., Jordà, G., Aznar, R., Déqué, M., Herrmann, M., Marcos, M., Dubois, C., Padorno, E., Alvarez-Fanjul, E., and Gomis, D.: Mediterranean Sea response to climate change in an ensemble of twenty first century scenarios, Climate Dynamics, 45, 2775–2802, https://doi.org/10.1007/S00382-015-2507-3/TABLES/8, 2015.

Ayache, M., Dutay, J.-C., Jean-Baptiste, P., Beranger, K., Arsouze, T., Beuvier, J., Palmieri, J., Le-Vu, B., and Roether, W.: Modelling of the anthropogenic tritium transient and its decay product helium-3 in the Mediterranean Sea using a high-resolution regional model, Ocean Science, 11, https://doi.org/10.5194/os-11-323-2015, 2015a.

Ayache, M., Dutay, J.-C., Jean-Baptiste, P., and Fourré, E.: Simulation of the mantle and crustal helium isotope signature in the Mediterranean Sea using a high-resolution regional circulation model, Ocean Science, 11, https://doi.org/10.5194/os-11-965-2015, 2015b.

Ayache, M., Dutay, J.-C., Arsouze, T., Révillon, S., Beuvier, J., and Jeandel, C.: High-resolution neodymium characterization along the Mediterranean margins and modelling of Nd distribution in the Mediterranean basins, Biogeosciences, 13, https://doi.org/10.5194/bg-13-5259-2016, 2016.

Ayache, M., Dutay, J.-C., Mouchet, A., Tisnérat-Laborde, N., Montagna, P., Tanhua, T., Siani, G., and Jean-Baptiste, P.: High-resolution regional modelling of natural and anthropogenic radiocarbon in the Mediterranean Sea, Biogeosciences, 14, https://doi.org/10.5194/bg-14-1197-2017, 2017.

Ayache, M., Dutay, J. C., Tachikawa, K., Arsouze, T., and Jeandel, C.: Neodymium budget in the Mediterranean Sea: evaluating the role of atmospheric dusts using a high-resolution dynamical-biogeochemical model, Biogeosciences, 20, 205–227, https://doi.org/10.5194/BG-20-205-2023, 2023.

Ayache, M., Dutay, J.-C., Mouchet, A., Tachikawa, K., Risi, C., and Ramstein, G.: Model and output for Ayache et al "Modelling the water isotopes distribution in the Mediterranean Sea using a high-resolution oceanic model (NEMO-MED12-watiso-v1.0): Evaluation of model results against in-situ observations ", Zenodo, https://doi.org/https://doi.org/10.5281/zenodo.10453745, 2024.

Barnier, B., Siefridt, L., and Marchesiello, P.: Thermal forcing for a global ocean circulation model using a three-year climatology of ECMWF analyses, Journal of Marine Systems, 6, 363–380, https://doi.org/10.1016/0924-7963(94)00034-9, 1995.

Bemis, B. E., Spero, H. J., Bijma, J., and Lea, D. W.: Reevaluation of the oxygen isotopic composition of planktonic foraminifera: Experimental results and revised paleotemperature equations, Paleoceanography, 13, 150–160, https://doi.org/10.1029/98PA00070, 1998.

Beuvier, J., Brossier, C. L., Béranger, K., Arsouze, T., Bourdallé-Badie, R., Deltel, C., Drillet, Y., Drobinski, P., Lyard, F., Ferry, N., Sevault, F., S, and Somot: MED12, Oceanic component for the modelling of the regional Mediterranean Earth System, Mercator Ocean Quarterly Newsletter, 46, 60–66, 2012a.

Beuvier, J., Béranger, K., Brossier, C. L., Somot, S., Sevault, F., Drillet, Y., Bourdallé-Badie, R., Ferry, N., and Lyard, F.: Spreading of the Western Mediterranean Deep Water after winter 2005: Time scales and deep cyclone transport, Journal of Geophysical Research, 117, C07 022, https://doi.org/10.1029/2011JC007679, 2012b.

Bigg, G. R., Jickells, T. D., Liss, P. S., and Osborn, T. J.: The role of the oceans in climate, International Journal of Climatology, 23, 1127–1159, https://doi.org/10.1002/JOC.926, 2003.

Bowen, G. J., Cai, Z., Fiorella, R. P., Putman, A. L., Bowen, G. J., Cai, Z., Fiorella, R. P., and Putman, A. L.: Isotopes in the Water Cycle: Regional- to Global-Scale Patterns and Applications, AREPS, 47, 453–479, https://doi.org/10.1146/ANNUREV-EARTH-053018-060220, 2019.

https://doi.org/10.5194/gmd-2023-237
Preprint. Discussion started: 10 January 2024

Bretherton, C. S. and Battisti, D. S.: An interpretation of the results from atmospheric general circulation models forced by the time history of the observed sea surface temperature distribution, Geophysical Research Letters, 27, 767–770, https://doi.org/10.1029/1999GL010910, 2000.

Brossier, C. L., Béranger, K., Deltel, C., and Drobinski, P.: The Mediterranean response to different space–time resolution atmospheric forcings using perpetual mode sensitivity simulations, Ocean Modelling, 36, 1–25, https://doi.org/10.1016/j.ocemod.2010.10.008, 2011.

Brown, J., Simmonds, I., and Noone, D.: Modeling δ18O in tropical precipitation and the surface ocean for present-day climate, Journal of Geophysical Research: Atmospheres, 111, 5105, https://doi.org/10.1029/2004JD005611, 2006.

Cauquoin, A., Werner, M., and Lohmann, G.: Water isotopes - Climate relationships for the mid-Holocene and preindustrial period simulated with an isotope-enabled version of MPI-ESM, Climate of the Past, 15, 1913–1937, https://doi.org/10.5194/CP-15-1913-2019, 2019.

Chelton, D. B., Schlax, M. G., and Samelson, R. M.: Global observations of nonlinear mesoscale eddies, Progress in Oceanography, 91, 167–216, https://doi.org/10.1016/J.POCEAN.2011.01.002, 2011.

Craig, H. and Gordon, L.: Deuterium and oxygen 18 variations in the ocean and the marine atmosphere, in: Proc. Stable Isotopes in Oceanographic Studies and Paleotemperatures, pp. 9–130, 1965.

Dansgaard, W.: Stable isotopes in precipitation, Tellus, 16, 468–468, 1964.

Delaygue, G., Jouzel, J., and Dutay, J. C.: Oxygen 18-salinity relationship simulated by an oceanic general circulation model, Earth and Planetary Science Letters, 178, 113–123, https://doi.org/10.1016/S0012-821X(00)00073-X, 2000.

Delaygue, G., Bard, E., Rollion, C., Jouzel, J., Stiévenard, M., Duplessy, J. C., and Ganssen, G.: Oxygen isotope/salinity relationship in the northern Indian Ocean, Journal of Geophysical Research: Oceans, 106, 4565–4574, https://doi.org/10.1029/1999JC000061, 2001.

Dong, C., McWilliams, J. C., Liu, Y., and Chen, D.: Global heat and salt transports by eddy movement, Nature Communications 2014 5:1, 5, 1–6, https://doi.org/10.1038/ncomms4294, 2014.

Epstein, S. and Mayeda, T.: Variation of O18 content of waters from natural sources, Geochimica et Cosmochimica Acta, 4, 213–224, https://doi.org/10.1016/0016-7037(53)90051-9, 1953.

Galewsky, J., Steen-Larsen, H. C., Field, R. D., Worden, J., Risi, C., and Schneider, M.: Stable isotopes in atmospheric water vapor and applications to the hydrologic cycle, Reviews of Geophysics, 54, 809–865, https://doi.org/10.1002/2015RG000512, 2016.

Gat, J. R., Bowser, C. J., and Kendall, C.: The contribution of evaporation from the Great Lakes to the continental atmosphere: estimate based on stable isotope data, Geophysical Research Letters, 21, 557–560, https://doi.org/10.1029/94GL00069, 1994.

Gat, J. R., Shemesh, A., Tziperman, E., Hecht, A., Georgopoulos, D., and Basturk, O.: The stable isotope composition of waters of the eastern Mediterranean Sea, Journal of Geophysical Research: Oceans, 101, 6441–6451, https://doi.org/10.1029/95JC02829, 1996.

Gat, R.: Oxygen and Hydrogen Isotopes in the Hydrologic Cycle, AREPS, 24, 225–262, https://doi.org/10.1146/ANNUREV.EARTH.24.1.225, 1996.

Grant, K. M., Grimm, R., Mikolajewicz, U., Marino, G., Ziegler, M., and Rohling, E. J.: The timing of Mediterranean sapropel deposition relative to insolation, sea-level and African monsoon changes, Quaternary Science Reviews, 140, 125–141, https://doi.org/10.1016/J.QUASCIREV.2016.03.026, 2016.

Guyennon, A., Baklouti, M., Diaz, F., Palmieri, J., Beuvier, J., Lebaupin-Brossier, C., Arsouze, T., Béranger, K., Dutay, J.-C., and Moutin, T.: New insights into the organic carbon export in the Mediterranean Sea from 3-D modeling, Biogeosciences, 12, 7025–7046, https://doi.org/10.5194/bg-12-7025-2015, 2015.

Herrmann, M., Sevault, F., Beuvier, J., and Somot, S.: What induced the exceptional 2005 convection event in the northwestern Mediterranean basin? Answers from a modeling study, Journal of Geophysical Research, 115, C12 051, https://doi.org/10.1029/2010JC006162, 2010.

https://doi.org/10.5194/gmd-2023-237
Preprint. Discussion started: 10 January 2024

Herrmann, M. J. and Somot, S.: Relevance of ERA40 dynamical downscaling for modeling deep convection in the Mediterranean Sea, Geophysical Research Letters, 35, L04 607, https://doi.org/10.1029/2007GL032442, 2008.

Hoffmann, G., Werner, M., and Heimann, M.: Water isotope module of the ECHAM atmospheric general circulation model: A study on timescales from days to several years, Journal of Geophysical Research: Atmospheres, 103, 16 871–16 896, https://doi.org/10.1029/98JD00423, 1998.

Hourdin, F., Ginus-Bogdan, A., Braconnot, P., Dufresne, J. L., Traore, A. K., and Rio, C.: Air moisture control on ocean surface temperature, hidden key to the warm bias enigma, Geophysical Research Letters, 42, 10,885–10,893, https://doi.org/10.1002/2015GL066764, 2015.

Jones, M. D. and Dee, S. G.: Global-scale proxy system modelling of oxygen isotopes in lacustrine carbonates: New insights from isotope-enabled-model proxy-data comparison, Quaternary Science Reviews, 202, 19–29, https://doi.org/10.1016/J.QUASCIREV.2018.09.009, 2018.

Joussaume, S., Sadourny, R., and Jouzel, J.: A general circulation model of water isotope cycles in the atmosphere, Nature 1984 311:5981, 311, 24–29, https://doi.org/10.1038/311024a0, 1984.

Jouzel, J., Russell, G. L., Suozzo, R. J., Koster, R. D., and White, J. W. C.: Simulations of the HDO and H2O-18 atmospheric cycles using the NASA GISS general circulation model - The seasonal cycle for present-day conditions, Journal of Geophysical Research, 92, 1987.

Juillet-Leclerc, A., Jouzel, J., Labeyrie, L., Joussaume, S., Juillet-Leclerc, A., Jouzel, J., Labeyrie, L., and Joussaume, S.: Modern and last glacial maximum sea surface δ ¹⁸O derived from an Atmospheric General Circulation Model, EPSL, 146, 591–605, https://doi.org/10.1016/S0012-821X(96)00237-3, 1997.

Kim, S. T. and O'Neil, J. R.: Equilibrium and nonequilibrium oxygen isotope effects in synthetic carbonates, Geochimica et Cosmochimica Acta, 61, 3461–3475, https://doi.org/10.1016/S0016-7037(97)00169-5, 1997.

Lascaratos, A., Roether, W., Nittis, K., and Klein, B.: Recent changes in deep water formation and spreading in the eastern Mediterranean Sea: a review, Progress in Oceanography, 44, 5–36, https://doi.org/10.1016/S0079-6611(99)00019-1, 1999.

Laube-Lenfant, E.: Utilisation des isotopes naturels 18o de l'eau et 13c du carbone inorganique dissous comme traceurs oceaniques dans les zones frontales et d'upwelling. Cas du pacifique equatorial et de la mer d'alboran, http://www.theses.fr, http://www.theses.fr/1996PA066229, 1996.

LeGrande, A. N. and Schmidt, G. A.: Global gridded data set of the oxygen isotopic composition in seawater, Geophysical Research Letters, 33, 12 604, https://doi.org/10.1029/2006GL026011, 2006.

Li, L., Bozec, A., Somot, S., Béranger, K., Bouruet-Aubertot, P., Sevault, F., and Crépon, M.: Chapter 7 Regional atmospheric, marine processes and climate modelling, Developments in Earth and Environmental Sciences, 4, 373–397, https://doi.org/10.1016/S1571-9197(06)80010-8, 2006.

Ludwig, W., Dumont, E., Meybeck, M., and Heussner, S.: River discharges of water and nutrients to the Mediterranean and Black Sea: Major drivers for ecosystem changes during past and future decades?, Progress in Oceanography, 80, 199–217, https://doi.org/10.1016/j.pocean.2009.02.001, 2009.

Madec, G. and NEMO-Team.: Note du Pole de modélisation, Institut Pierre-Simon Laplace (IPSL), France, NEMO ocean engine, 27, https://doi.org/ISSN N1288-1619, 2008.

Mariotti, A., Zeng, N., and Lau, K. M.: Euro-Mediterranean rainfall and ENSO—a seasonally varying relationship, Geophysical Research Letters, 29, 59–1, https://doi.org/10.1029/2001GL014248, 2002.

Millot, C. and Taupier-Letage, I.: The Mediterranean Sea, vol. 5K, https://doi.org/10.1007/b107143., 2005.

https://doi.org/10.5194/gmd-2023-237
Preprint. Discussion started: 10 January 2024

Mook, W. G., Bommerson, J. C., Staverman, W. H., Mook, W. G., Bommerson, J. C., and Staverman, W. H.: Carbon isotope fractionation between dissolved bicarbonate and gaseous carbon dioxide, EPSL, 22, 169–176, https://doi.org/10.1016/0012-821X(74)90078-8, 1974.

Pagès, R., Baklouti, M., Barrier, N., Ayache, M., Sevault, F., Somot, S., and Moutin, T.: Projected Effects of Climate-Induced Changes in Hydrodynamics on the Biogeochemistry of the Mediterranean Sea Under the RCP 8.5 Regional Climate Scenario, Frontiers in Marine Science, 7, 563 615, https://doi.org/10.3389/FMARS.2020.563615/BIBTEX, 2020.

Palmiéri, J., Orr, J. C., Dutay, J.-C., Béranger, K., Schneider, A., Beuvier, J., and Somot, S.: Simulated anthropogenic CO2 storage and acidification of the Mediterranean Sea, Biogeosciences, 12, 781–802, https://doi.org/10.5194/bg-12-781-2015, 2015.

Paul, A., Mulitza, S., Pätzold, J., and Wolff, T.: Simulation of Oxygen Isotopes in a Global Ocean Model, Use of Proxies in Paleoceanography, pp. 655–686, https://doi.org/10.1007/978-3-642-58646-0_27, 1999.

Pfahl, S. and Wernli, H.: Air parcel trajectory analysis of stable isotopes in water vapor in the eastern Mediterranean, Journal of Geophysical Research: Atmospheres, 113, 20 104, https://doi.org/10.1029/2008JD009839, 2008.

Pierre, C.: The oxygen and carbon isotope distribution in the Mediterranean water masses, Marine Geology, 153, 41–55, https://doi.org/10.1016/S0025-3227(98)00090-5, 1999.

Pierre, C., Vergnaud-Grazzini, C., Thouron, D., and Saliège, J.-F.: Compositions isotopiques de l'oxygène et du carbone des masses d'eau en Méditerranée, Memorie della Societa Geologica Italiana, 36, 165–174, 1986.

Pinardi, N. and Masetti, E.: Variability of the large scale general circulation of the Mediterranean Sea from observations and modelling: A review, Palaeogeography, Palaeoclimatology, Palaeoecology, 158, 153–173, https://doi.org/10.1016/S0031-0182(00)00048-1, 2000.

Richon, C., Dutay, J. C., Dulac, F., Wang, R., and Balkanski, Y.: Modeling the biogeochemical impact of atmospheric phosphate deposition from desert dust and combustion sources to the Mediterranean Sea, Biogeosciences, 15, 2499–2524, https://doi.org/10.5194/BG-15-2499-2018, 2018.

Richon, C., Dutay, J. C., Bopp, L., Vu, B. L., Orr, J. C., Somot, S., and Dulac, F.: Biogeochemical response of the Mediterranean Sea to the transient SRES-A2 climate change scenario, Biogeosciences, 16, 135–165, https://doi.org/10.5194/BG-16-135-2019, 2019.

Risi, C., Bony, S., Vimeux, F., Chongd, M., and Descroixe, L.: Evolution of the stable water isotopic composition of the rain sampled along Sahelian squall lines, Quarterly Journal of the Royal Meteorological Society, 136, 227–242, https://doi.org/10.1002/QJ.485, 2010a.

Risi, C., Bony, S., Vimeux, F., and Jouzel, J.: Water-stable isotopes in the LMDZ4 general circulation model: Model evaluation for present-day and past climates and applications to climatic interpretations of tropical isotopic records, Journal of Geophysical Research: Atmospheres, 115, 12 118, https://doi.org/10.1029/2009JD013255, 2010b.

Risi, C., Noone, D., Worden, J., Frankenberg, C., Stiller, G., Kiefer, M., Funke, B., Walker, K., Bernath, P., Schneider, M., Bony, S., Lee, J., Brown, D., and Sturm, C.: Process-evaluation of tropospheric humidity simulated by general circulation models using water vapor isotopic observations: 2. Using isotopic diagnostics to understand the mid and upper tropospheric moist bias in the tropics and subtropics, Journal of Geophysical Research: Atmospheres, 117, 5304, https://doi.org/10.1029/2011JD016623, 2012.

Risi, C., Noone, D., Frankenberg, C., and Worden, J.: Role of continental recycling in intraseasonal variations of continental moisture as deduced from model simulations and water vapor isotopic measurements, Water Resources Research, 49, 4136–4156, https://doi.org/10.1002/WRCR.20312, 2013.

Risi, C., Ogée, J., Bony, S., Bariac, T., Raz-Yaseef, N., Wingate, L., Welker, J., Knohl, A., Kurz-Besson, C., Leclerc, M., Zhang, G., Buchmann, N., Santrucek, J., Hronkova, M., David, T., Peylin, P., and Guglielmo, F.: The water isotopic version of the land-surface model ORCHIDEE: implementation, evaluation, sensitivity to hydrological parameters, Hydrol Current Res, 7, 4, https://doi.org/10.4172/2157-7587.1000258, 2016.

https://doi.org/10.5194/gmd-2023-237
Preprint. Discussion started: 10 January 2024

Roche, D., Paillard, D., Ganopolski, A., and Hoffmann, G.: Oceanic oxygen-18 at the present day and LGM: equilibrium simulations with a coupled climate model of intermediate complexity, Earth and Planetary Science Letters, 218, 317–330, https://doi.org/10.1016/S0012-821X(03)00700-3, 2004.

Roche, D. M. and Caley, T.: ?18O water isotope in the iLOVECLIM model (version 1.0) - Part 2: Evaluation of model results against observed ?18O in water samples, Geoscientific Model Development, 6, 1493–1504, https://doi.org/10.5194/GMD-6-1493-2013, 2013.

Rohling, E. J., Marino, G., and Grant, K. M.: Mediterranean climate and oceanography, and the periodic development of anoxic events (sapropels), https://doi.org/10.1016/j.earscirev.2015.01.008, 2015.

Schmidt, G. A.: Oxygen-18 variations in a global ocean model, Geophysical Research Letters, 25, 1201–1204, https://doi.org/10.1029/98GL50866, 1998.

Schmidt, G. A.: Forward modeling of carbonate proxy data from planktonic foraminifera using oxygen isotope tracers in a global ocean model, Paleoceanography, 14, 482–497, https://doi.org/10.1029/1999PA900025, 1999.

Schmidt, G. A., LeGrande, A. N., and Hoffmann, G.: Water isotope expressions of intrinsic and forced variability in a coupled ocean-atmosphere model, Journal of Geophysical Research Atmospheres, 112, https://doi.org/10.1029/2006JD007781, 2007.

Shackleton, N.: Oxygen Isotope Analyses and Pleistocene Temperatures Re-assessed, Nature 1967 215:5096, 215, 15–17, https://doi.org/10.1038/215015a0, 1967.

Shi, X., Cauquoin, A., Lohmann, G., Jonkers, L., Wang, Q., Yang, H., Sun, Y., and Werner, M.: Simulated stable water isotopes during the mid-Holocene and pre-industrial periods using AWI-ESM-2.1-wiso, Geoscientific Model Development, 16, 5153–5178, https://doi.org/10.5194/GMD-16-5153-2023, 2023.

Somot, S., Sevault, F., and Déqué, M.: Transient climate change scenario simulation of the Mediterranean Sea for the twenty-first century using a high-resolution ocean circulation model, Climate Dynamics, 27, 851–879, https://doi.org/10.1007/s00382-006-0167-z, 2006.

Soto-Navarro, C., Ravilious, C., Arnell, A., Lamo, X. D., Harfoot, M., Hill, S. L., Wearn, O. R., Santoro, M., Bouvet, A., Mermoz, S., Toan, T. L., Xia, J., Liu, S., Yuan, W., Spawn, S. A., Gibbs, H. K., Ferrier, S., Harwood, T., Alkemade, R., Schipper, A. M., Schmidt-Traub, G., Strassburg, B., Miles, L., Burgess, N. D., and Kapos, V.: Mapping co-benefits for carbon storage and biodiversity to inform conservation policy and action, Philosophical Transactions of the Royal Society B, 375, https://doi.org/10.1098/RSTB.2019.0128, 2020.

Soto-Navarro, J., Somot, S., Sevault, F., Beuvier, J., Béranger, K., Criado-Aldeanueva, F., and García-Lafuente, J.: Evaluation of regional ocean circulation models for the Mediterranean Sea at the Strait of Gibraltar : volume transport and thermohaline properties of the outflow, Climate Dynamics, https://doi.org/10.1007/s00382-014-2179-4, 2014.

Stahl, W. and Rinow, U.: Sauerstoffisotopenanalysen an Mittelmeerwässern : ein Beitrag zur Problematik von Paläotemperaturbestimmungen, 1973.

Stanev, E. V. and Peneva, E. L.: Regional sea level response to global climatic change : Black Sea examples, Europe, 32, 33 – 47, 2002.

Team, C. P.: Mod{é}lisation {à} haute r{é}solution de la circulation dans l'oc{é}an Atlantique forc{é}e et coupl{é}e oc{é}an-atmosph{é}re, Sci. Tech. Rep. CLIPPER-R3-99, Ifremer, Brest, France., 1999.

Tindall, J., Flecker, R., Valdes, P., Schmidt, D. N., Markwick, P., and Harris, J.: Modelling the oxygen isotope distribution of ancient seawater using a coupled ocean–atmosphere GCM: Implications for reconstructing early Eocene climate, Earth and Planetary Science Letters, 292, 265–273, https://doi.org/10.1016/J.EPSL.2009.12.049, 2010.

Vadsaria, T., Ramstein, G., Dutay, J. C., Li, L., Ayache, M., and Richon, C.: Simulating the Occurrence of the Last Sapropel Event (S1): Mediterranean Basin Ocean Dynamics Simulations Using Nd Isotopic Composition Modeling, Paleoceanography and Paleoclimatology, 34, 237–251, https://doi.org/10.1029/2019PA003566, 2019.

https://doi.org/10.5194/gmd-2023-237
Preprint. Discussion started: 10 January 2024

Vadsaria, T., Li, L., Ramstein, G., and Dutay, J. C.: Development of a sequential tool, LMDZ-NEMO-med-V1, to conduct global-to-regional past climate simulation for the Mediterranean basin: an Early Holocene case study, Geoscientific Model Development, 13, 2337–2354, https://doi.org/10.5194/GMD-13-2337-2020, 2020.

Vörösmarty, C. J., Fekete, B. M., and Tucker, B. A.: Global River Discharge Database (RivDIS V1.0), International Hydrological Program, Global Hydrological Archive and Analysis Systems, UNESCO, Paris, 1996.

Wadley, M. R., Bigg, G. R., Rohling, E. J., and Payne, A. J.: On modelling present-day and last glacial maximum oceanic δ18O distributions, Global and Planetary Change, 32, 89–109, https://doi.org/10.1016/S0921-8181(01)00084-4, 2002.

Werner, M., Langebroek, P. M., Carlsen, T., Herold, M., and Lohmann, G.: Stable water isotopes in the ECHAM5 general circulation model: Toward high-resolution isotope modeling on a global scale, Journal of Geophysical Research: Atmospheres, 116, 15 109, https://doi.org/10.1029/2011JD015681, 2011.

Werner, M., Haese, B., Xu, X., Zhang, X., Butzin, M., and Lohmann, G.: Glacial-interglacial changes in H 2 O, HDO and deuterium excess-results from the fully coupled ECHAM5/MPI-OM Earth system model, Geosci. Model Dev, 9, 647–670, https://doi.org/10.5194/gmd-9-647-2016, 2016.

Xu, X., Werner, M., Butzin, M., and Lohmann, G.: Water isotope variations in the global ocean model MPI-OM, Geoscientific Model Development, 5, 809–818, https://doi.org/10.5194/GMD-5-809-2012, 2012.

https://doi.org/10.5194/gmd-2023-237
Preprint. Discussion started: 10 January 2024

Geoscientific Model Development Discussions

Acknowledgements. The research leading to this study has received funding from the French National Research Agency ANR project MedSens. The LMDZ-iso simulation was performed using the HPC resources of IDRIS under the allocation AD010107632 made by GENCI.

Code availability. The source code of NEMO and LMDZiso models are available from the project website: https://forge.ipsl.jussieu.fr/igcmg_doc/wiki/Doc/Models/NEMO (last access: July 2023), and https://forge.ipsl.jussieu.fr/igcmg_doc/wiki/Doc/Models/LMDZ (last accessed: July 2023) under the terms of the CeCill license for both LMDZ and NEMO. The exact version of the model used to produce the results reported in this paper is archived on Zenodo (https://doi.org/10.5281/zenodo.10453745) (Ayache et al., 2024, see supplement).

Data availability. The data associated with the paper are available from the corresponding author upon request. All of the data used in this study were published by their authors as cited in the paper.

Author contributions. MA, JCD, AM contributed to the model development, simulations, and diagnostics. MA, JCD, KT, CA, GR were involved in the writing and revision of the manuscript.

Competing interests. The authors declare that they have no conflict of interest

Table 1. Mean, standard deviation, minimum and maximum values from the model outputs and available in-situ data from (Epstein and Mayeda, 1953; Stahl and Rinow, 1973; Pierre et al., 1986; Gat et al., 1996; Pierre, 1999) calculated in the surface water (0-100 m depth) of the whole basin, eastern, and western basins.

		Model	In-situ data
Whole basin	Mean	1.55	1.46
	Min	0.74	0.7
	Max	1.82	2.19
	Std	0.2	0.25
WMed	Mean	1.4	1.2
	Min	0.74	0.7
	Max	1.71	1.67
	Std	0.15	0.2
EMed	Mean	1.68	1.57
	Min	0.8	1.19
	Max	1.82	2.19
	Std	0.12	0.18

https://doi.org/10.5194/gmd-2023-237
Preprint. Discussion started: 10 January 2024

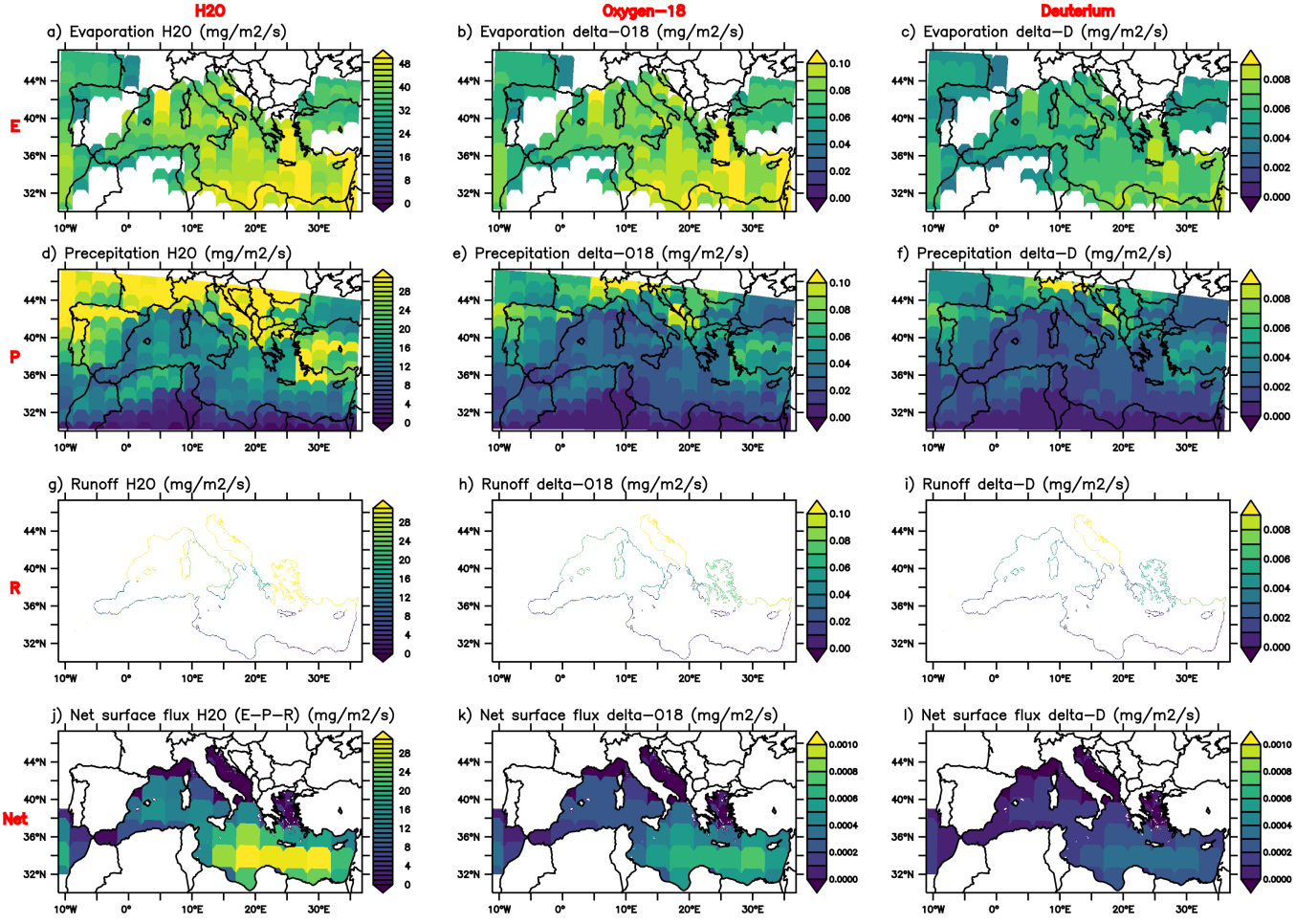

Figure 1. Boundary conditions and input (evaporation and precipitation) maps applied to NEMO that originate from the LMDZ-iso atmospheric model (Risi et al., 2010b).**a)** Evaporation, **b)** Precepitaion, **c)** River runoff, **J)** Net surface flux (E - P - R) for H_2O, **(b, e, h, k)** the same but for $\delta^{18}O_{sw}$, **(c, f, i, l)** for δD . The isotopic composition of river runoff is not available from the LMDZ-iso model: this flux is computed as ^{18}RP × R where R is prepared from the data ofLudwig et al. (2009) and Vörösmarty et al. (1996) and ^{18}RP is the isotopic ratio in precipitations at the same time and location

https://doi.org/10.5194/gmd-2023-237
Preprint. Discussion started: 10 January 2024

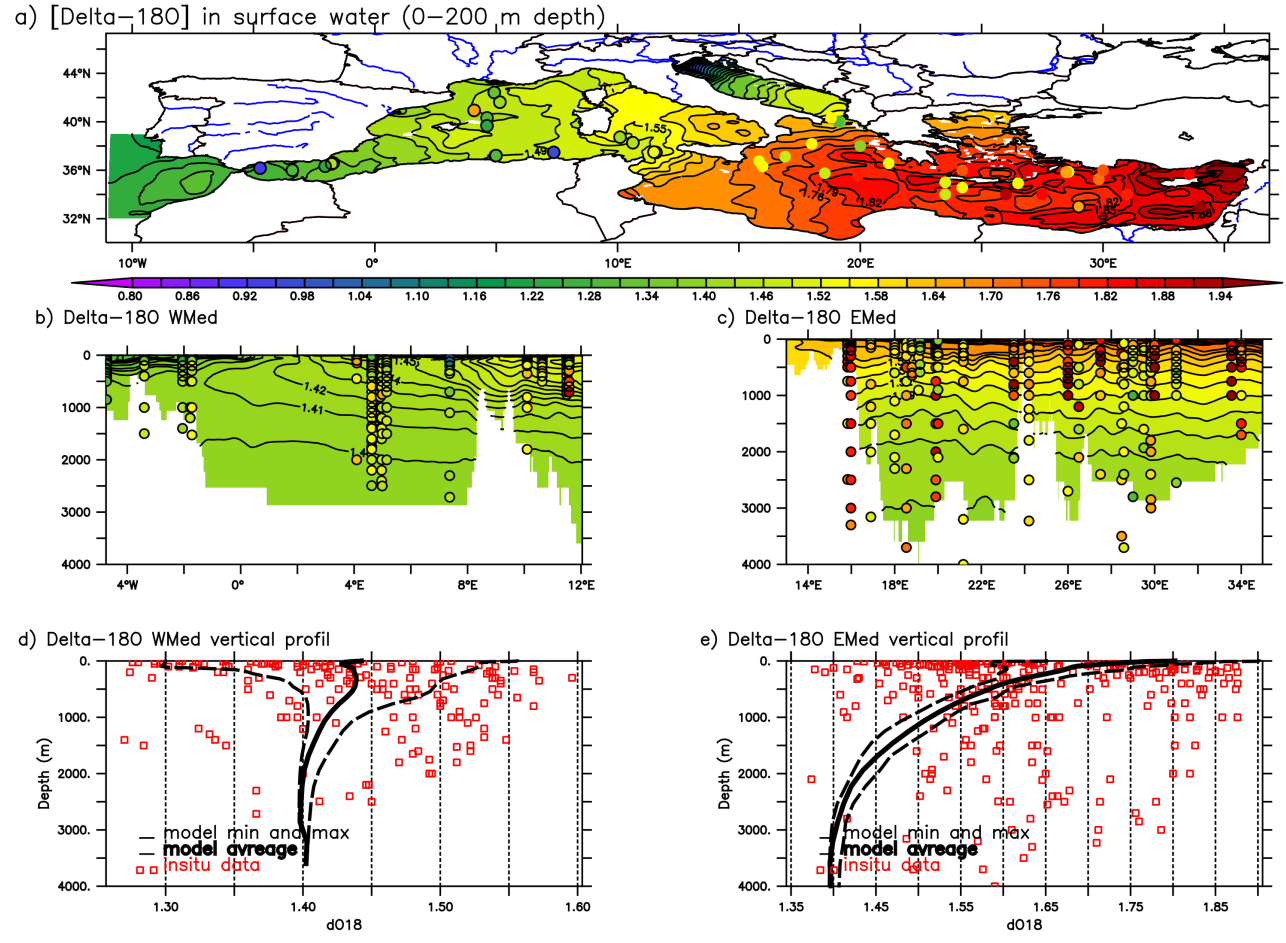

Figure 2. The model outputs against in-situ data for the present-day situation. **a)** $\delta^{18}O_{sw}$ (in ‰) distribution in the surface water (50 m depth). **b)** E-W vertical section of $\delta^{18}O_{sw}$ (in ‰) in the western Mediterranean basin d) Zonal mean comparison of $\delta^{18}O_{sw}$ (in ‰) average vertical profiles in the western basin presenting model results against in-situ data. **c)** and **e)** the same as **b)** and **d)** but for the eastern basin. Colour filled dots represent in-situ observations from (Epstein and Mayeda, 1953; Stahl and Rinow, 1973; Pierre et al., 1986; Gat et al., 1996; Pierre, 1999). Both model and in-situ data use the same colour scale.

https://doi.org/10.5194/gmd-2023-237
Preprint. Discussion started: 10 January 2024

Geoscientific Model Development Discussions
Open Access
EGU

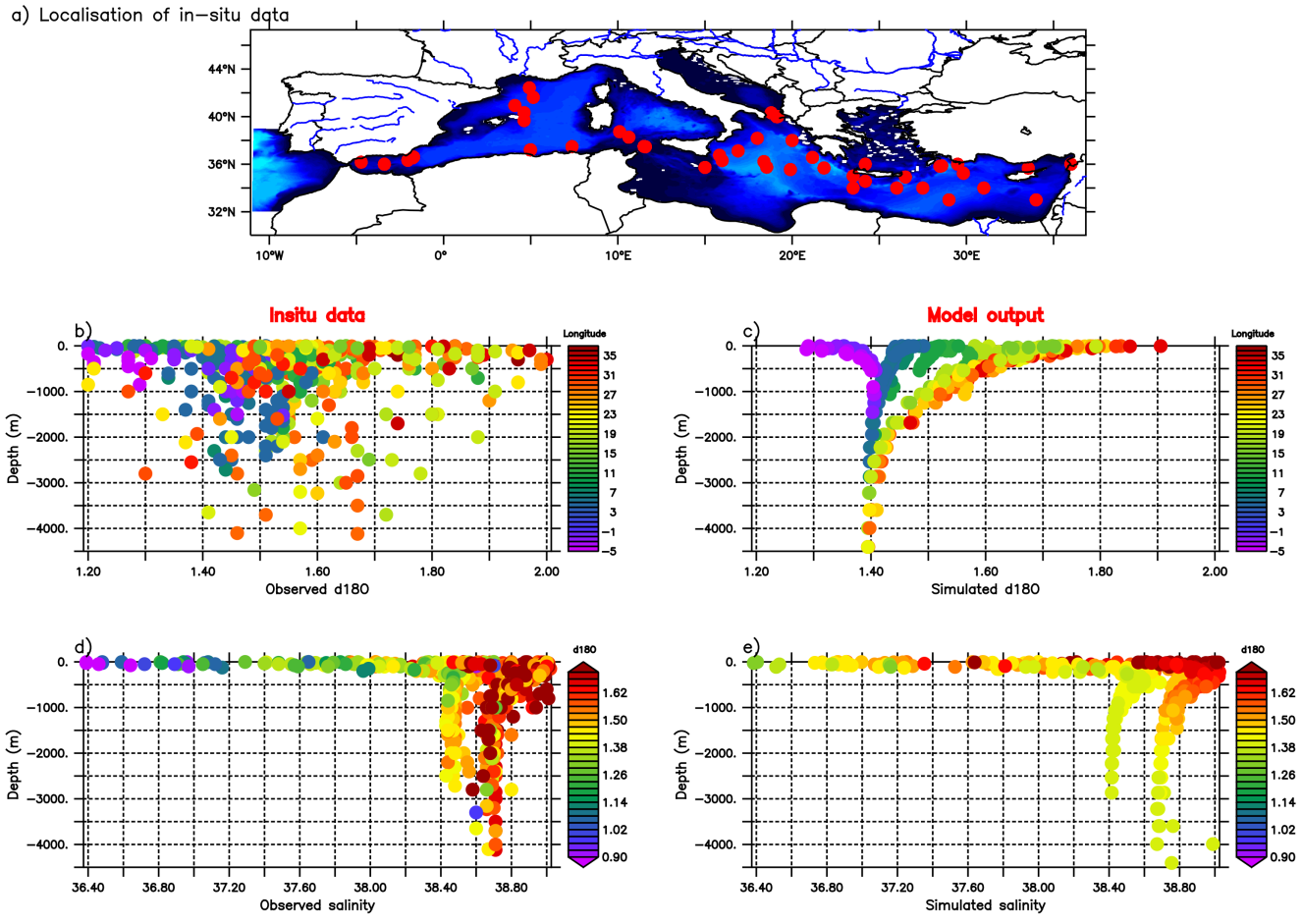

Figure 3. a) Location map of all stations of in-situ data (Epstein and Mayeda, 1953; Stahl and Rinow, 1973; Pierre et al., 1986; Gat et al., 1996; Pierre, 1999). **b)** depth profiles of the $\delta^{18}O_{sw}$ (in ‰) from in-situ data (the colour code indicates the latitudes of the data in °E). **c)** The same as in **b)** but from the model output. **d)** Depth profiles of salinity from in-situ observations (the colour code indicates the $\delta^{18}O_{sw}$ for each data station). **e)** The same as in **d)** but from the model output.

https://doi.org/10.5194/gmd-2023-237
Preprint. Discussion started: 10 January 2024

Geoscientific Model Development Discussions

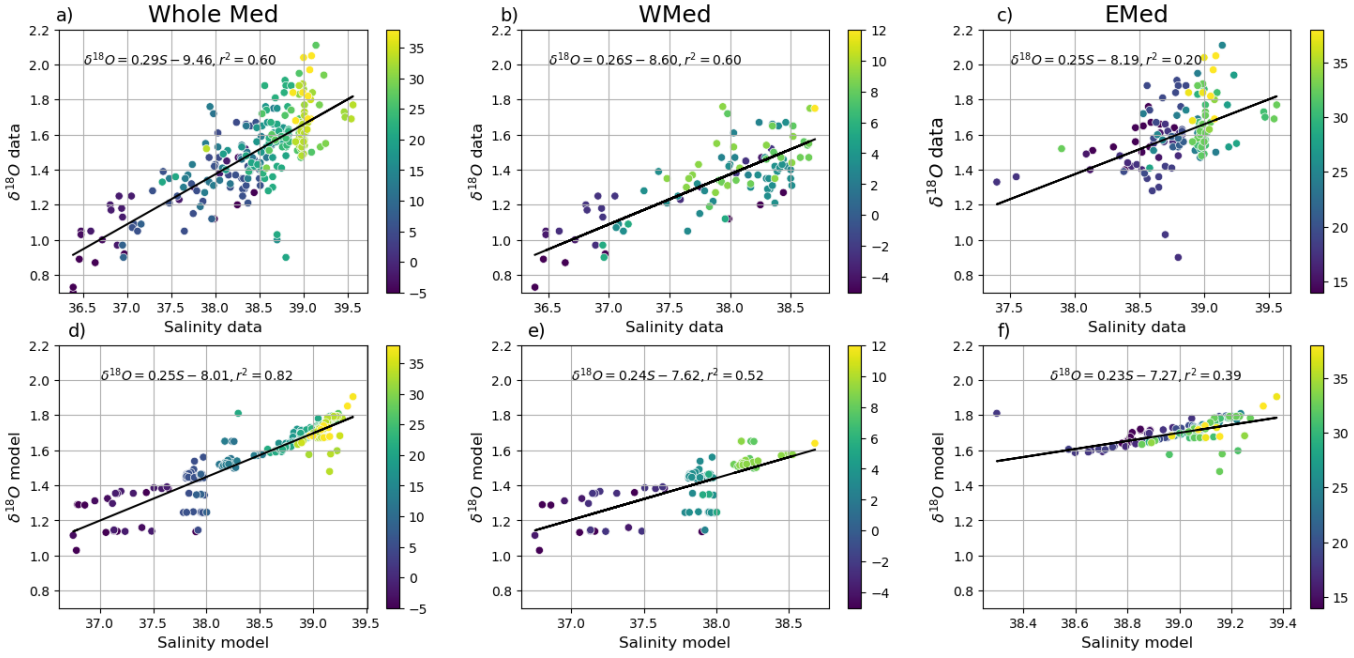

Figure 4. $\delta^{18}O_{sw}$–salinity relationship in the surface water (Average 0-200 m depth of the whole basin (left column), western basin (middle column), and of the eastern Mediterranean basin (right column) calculated from available in-situ data (Epstein and Mayeda, 1953; Stahl and Rinow, 1973; Pierre et al., 1986; Gat et al., 1996; Pierre, 1999) in the upper panel (in a, b, c), and from model outputs extracted in the same positions of in-situ data (in d, e, f). The colour code indicates the latitudes of the data in °E.

https://doi.org/10.5194/gmd-2023-237
Preprint. Discussion started: 10 January 2024

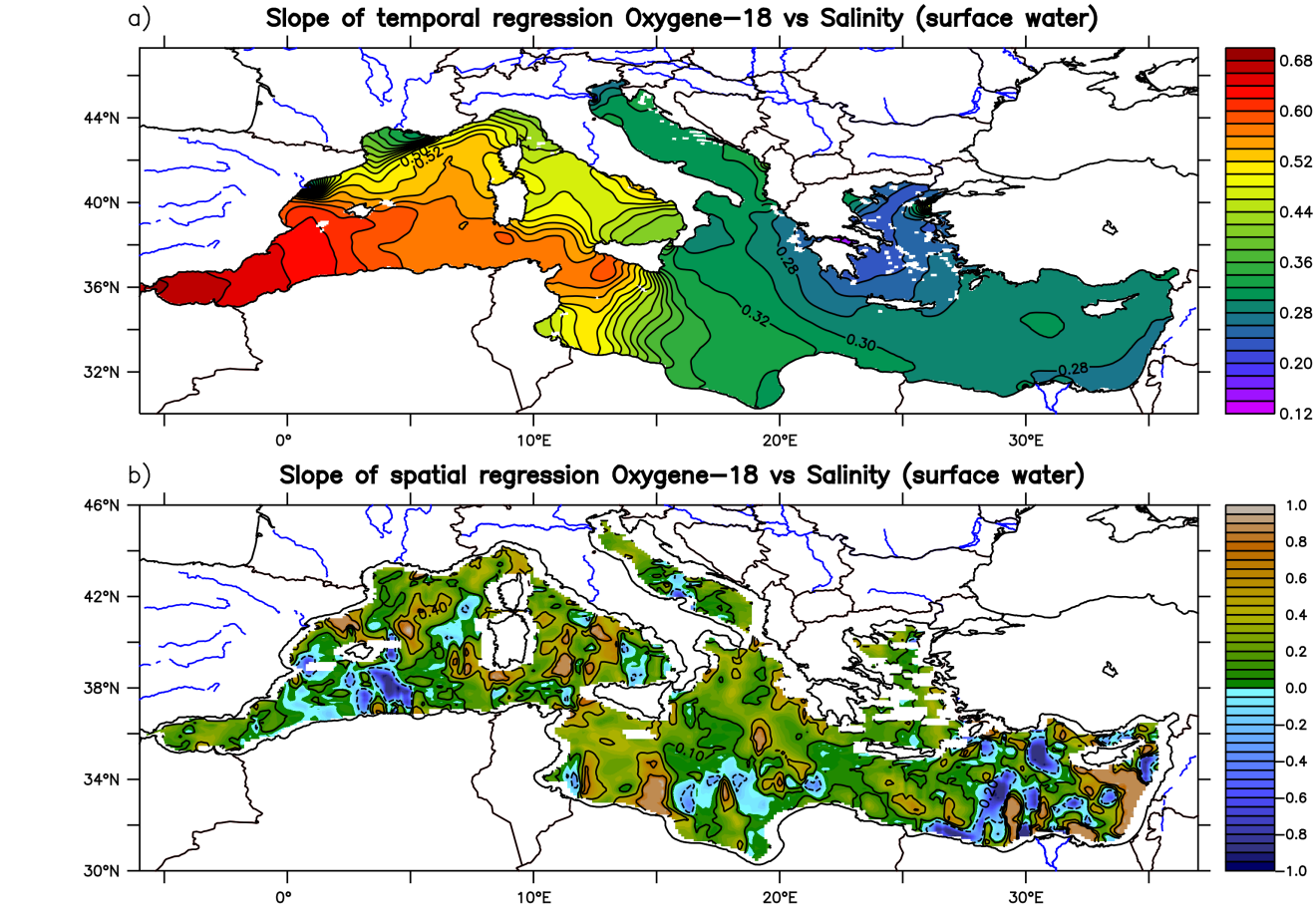

Figure 5. a) Horizontal map of slope of temporal regression between the $\delta^{18}O_{sw}$–salinity in the surface water computed using simulated last 30 years climatology, b) Spatial $\delta^{18}O_{sw}$-salinity slope from the model outputs calculated for each grid point using simulated surface values from the 12 surrounding grid points. The non-significant zones for the regression at 95% level are marked with a black cross.

https://doi.org/10.5194/gmd-2023-237
Preprint. Discussion started: 10 January 2024

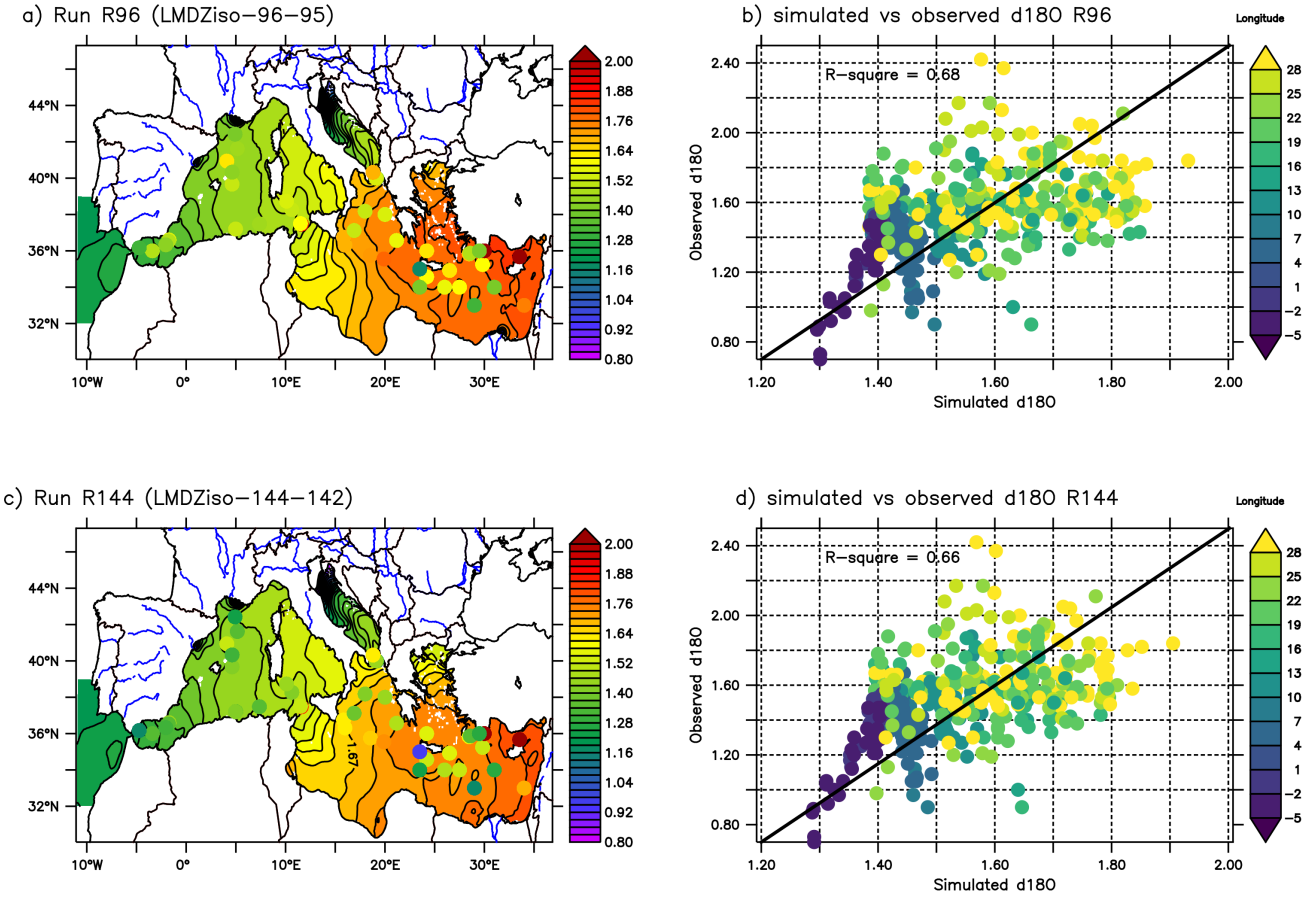

Figure 6. a) $\delta^{18}O_{sw}$ (in ‰) distribution in the surface water (50 m depth) from R96 simulation. Colour filled dots represent in-situ observations from (Epstein and Mayeda, 1953; Stahl and Rinow, 1973; Pierre et al., 1986; Gat et al., 1996; Pierre, 1999) , **b)** multi-scatter plot of simulated $\delta^{18}O_{sw}$ (averaged over last 30 years of the simulation) from R96 simulation versus in-situ data from (Epstein and Mayeda, 1953; Stahl and Rinow, 1973; Pierre et al., 1986; Gat et al., 1996; Pierre, 1999) in the whole basin. The colour code indicates the latitudes of the data in °E). **c)** and **d)** The same for a) and b) but from the R144 simulation.

https://doi.org/10.5194/gmd-2023-237
Preprint. Discussion started: 10 January 2024

Geoscientific Model Development
Discussions
Open Access
EGU

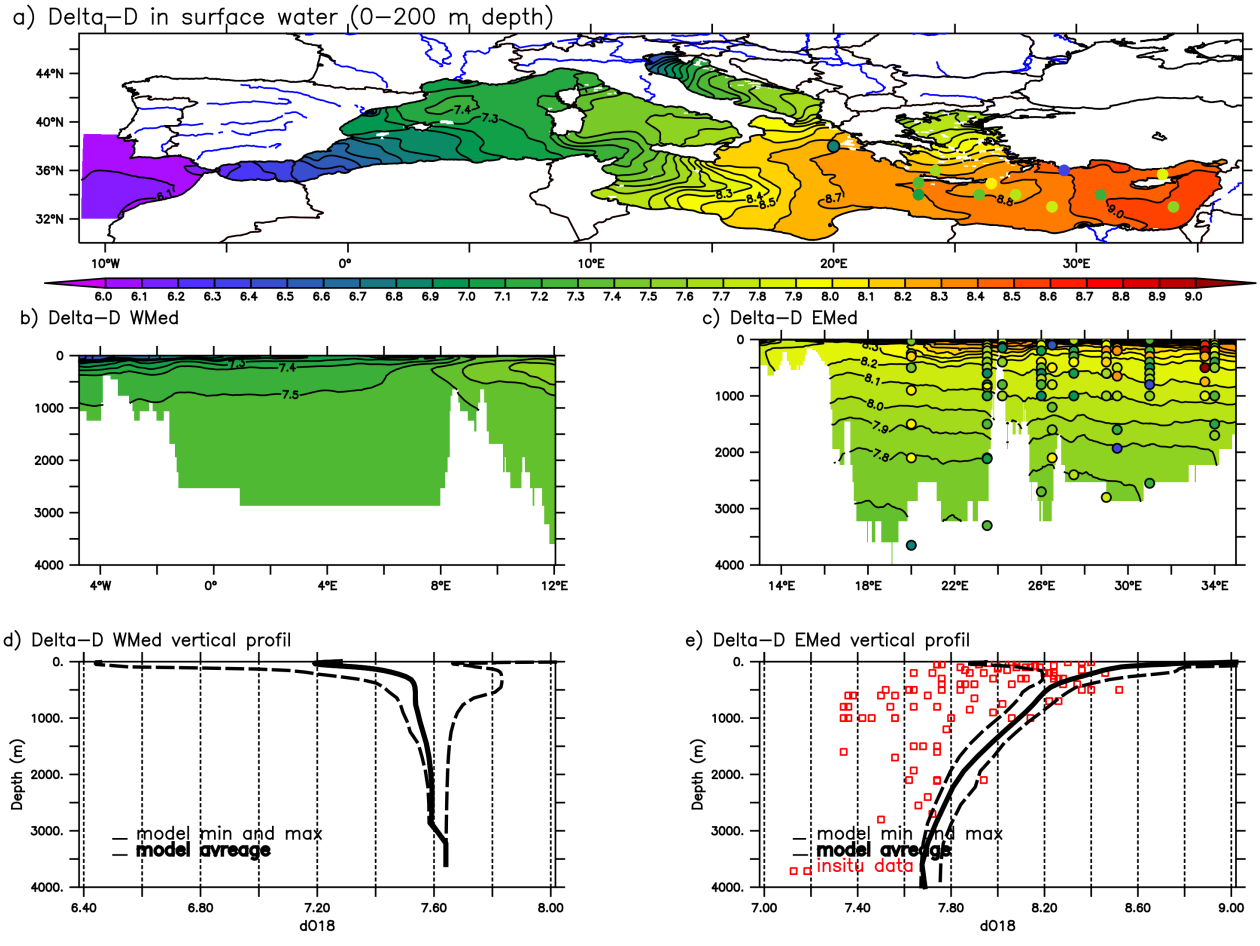

Figure 7. The same as in Fig. 2 but for Deuterium isotope (in ‰).

https://doi.org/10.5194/gmd-2023-237
Preprint. Discussion started: 10 January 2024

Geoscientific Model Development
Discussions
Open Access
EGU

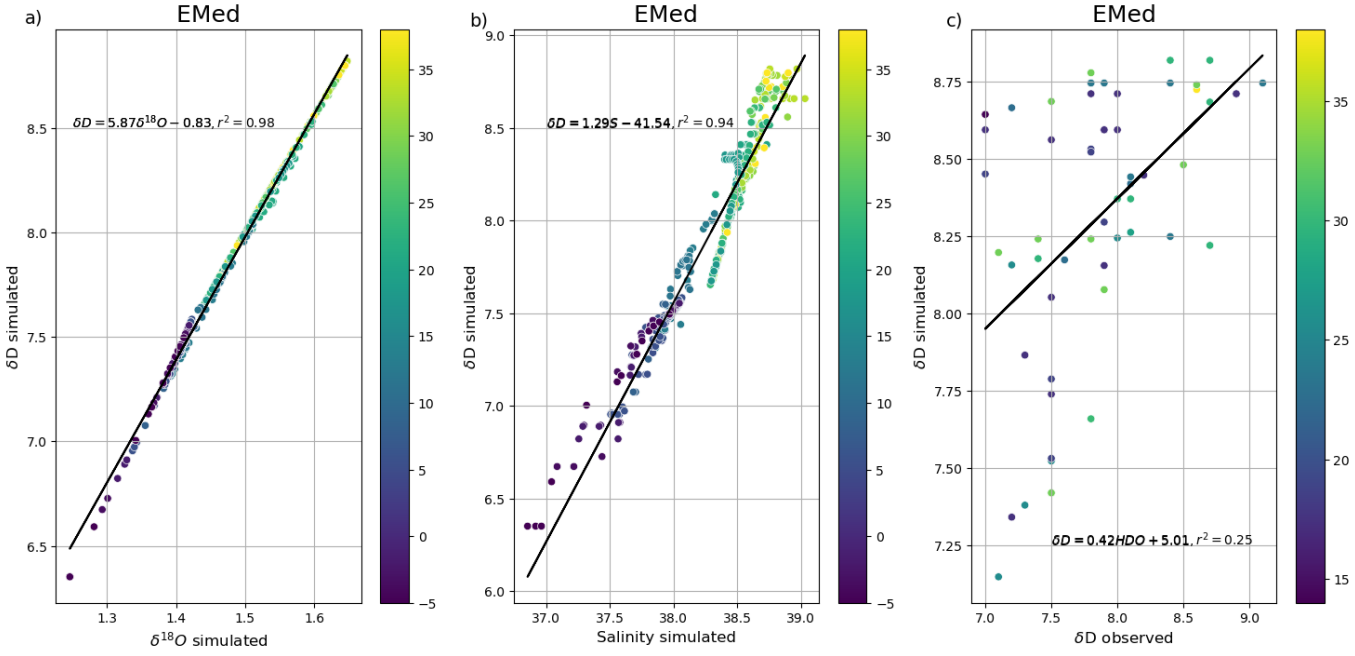

Figure 8. a) Multi-scatter plot of simulated $\delta^{18}O_{sw}$ (averaged over the last 30 years of the simulation) versus simulated δD at the same location of in-situ data in the eastern basin (left panel), b) simulated salinity versus simulated δD (middle panel), and observed δD (from Gat et al. (1996) against simulated δD in c) (right panel). The colour code indicates the latitudes of the data in °E.

https://doi.org/10.5194/gmd-2023-237
Preprint. Discussion started: 10 January 2024

Geoscientific Model Development Discussions
Open Access
EGU

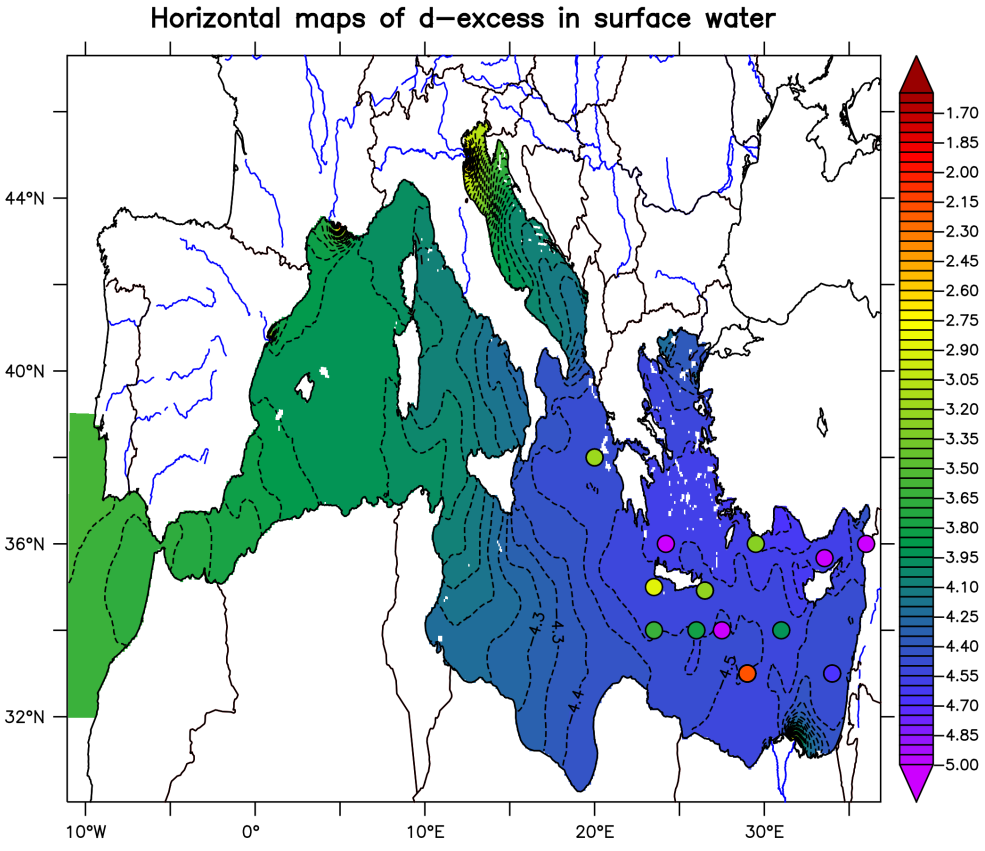

Figure 9. Horizontal map of d-excess in the surface water defined as deuterium excess (d-excess= δD – 8* $\delta^{18}O_{sw}$, Dansgaard (1964)). Colour filled dots represent in-situ observations from (Gat et al., 1996). Both model and in-situ data use the same colour scale.

https://doi.org/10.5194/gmd-2023-237
Preprint. Discussion started: 10 January 2024

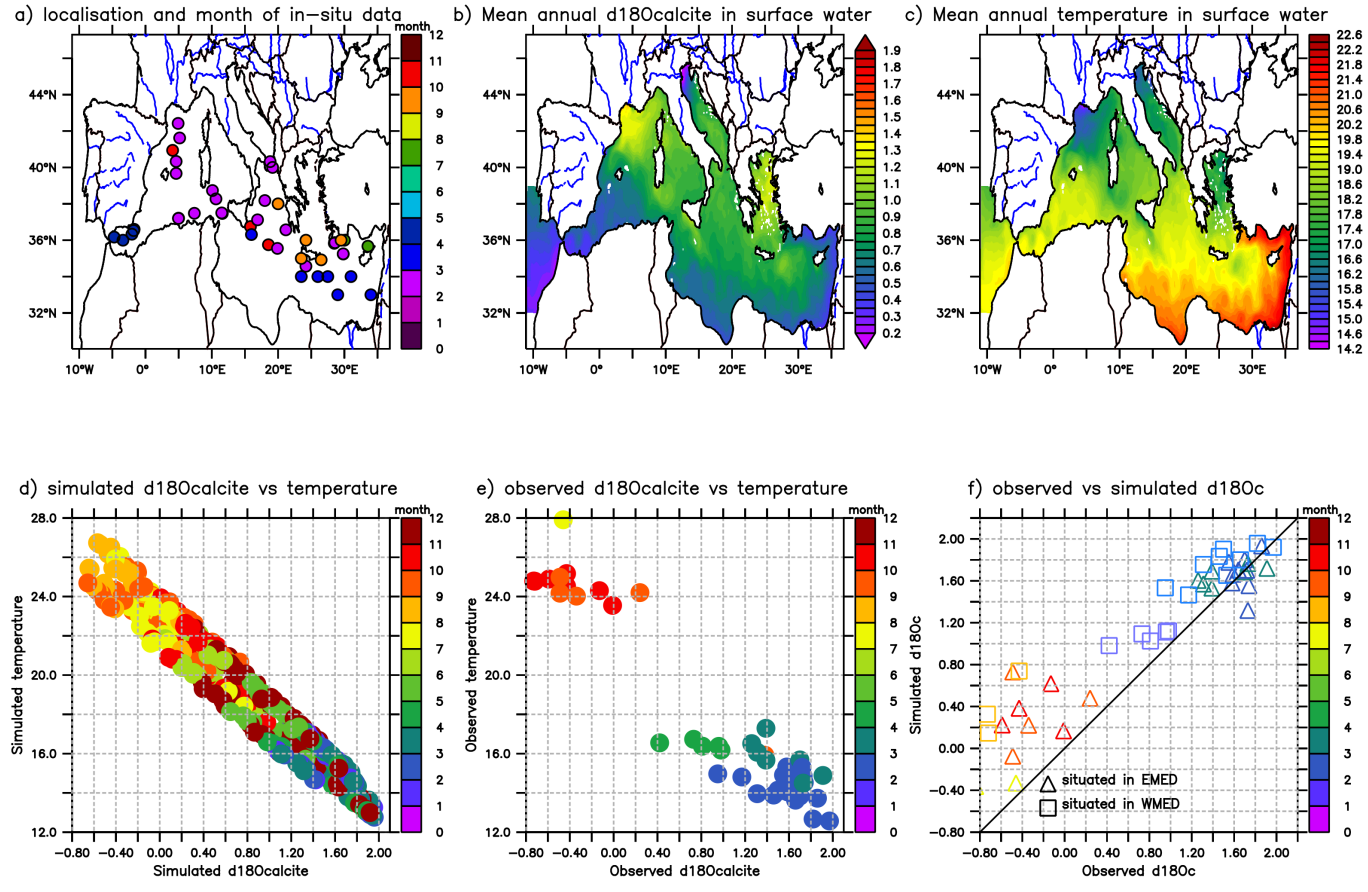

Figure 10. a) Localisation and the month of available in-situ data. b) Annual mean $\delta^{18}O_c$ (in ‰) distribution in calcite (surface layer 0-100 m depth), calculated using the method of Bemis and Howard, (1998). c) Horizontal maps of surface mean annual temperature in °C. d) Multi-scatter plots of simulated $\delta^{18}O_c$ against simulated temperature in the same location; the colour code shows months. e) the same as d) but from in-situ data. f) Comparison of the simulated and observed $\delta^{18}O_c$ (in ‰) in surface layer averaged in the two basins (boxes from the WMed and triangles from the EMed dashed line model). The colour code shows months.

https://doi.org/10.5194/gmd-2023-237
Preprint. Discussion started: 10 January 2024

Geoscientific Model Development Discussions
Open Access
EGU

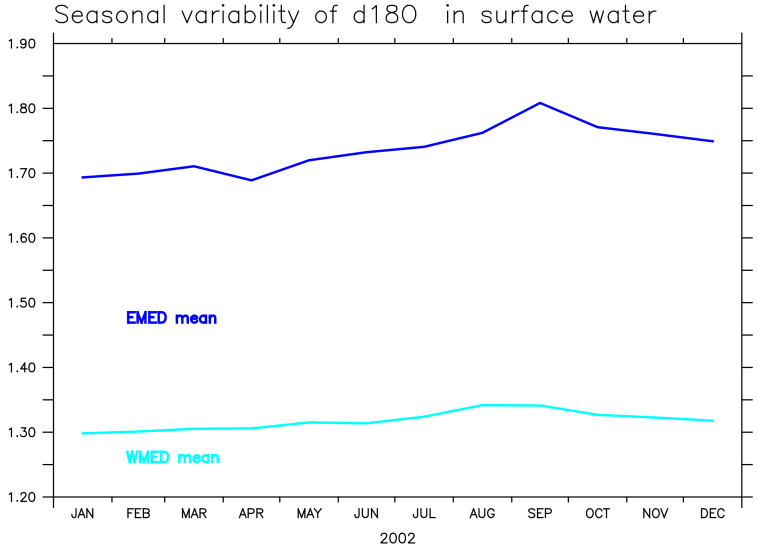

Figure A1. Seasonal variation of $\delta^{18}O_{sw}$ (in $‰$) in eastern and western basin surface waters

https://doi.org/10.5194/gmd-2023-237
Preprint. Discussion started: 10 January 2024

Geoscientific Model Development Discussions
Open Access
EGU

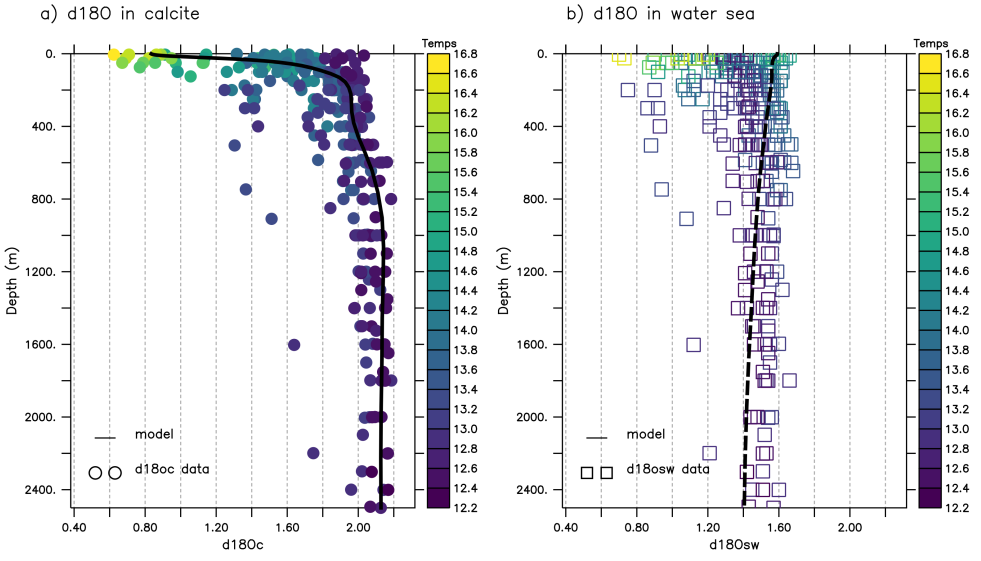

Figure A2. a) Comparaison of the simulated avreage vetical profiles of $\delta^{18}O_c$ (in ‰) (circle data and line from model outputs). b) same as a) but for $\delta^{18}O_{sw}$